# EMBEDMENT OF HYDROXYAPATITE (HA) ON TITANIUM ALLOY (Ti6Al4V) VIA SUPERPLASTIC DEFORMATION METHOD FOR MEDICAL APPLICATION

**HIDAYAH BINTI MOHD KHALID**

**FACULTY OF ENGINEERING**
**UNIVERSITY OF MALAYA**
**KUALA LUMPUR**

**2011**

# EMBEDMENT OF HYDROXYAPATITE (HA) ON TITANIUM ALLOY (Ti6Al4V) VIA SUPERPLASTIC DEFORMATION METHOD FOR MEDICAL IMPLANT

**HIDAYAH BINTI MOHD KHALID**

**DISSERTATION SUBMITTED IN FULFILLMENT OF THE REQUIREMENTS FOR THE DEGREE OF MASTER OF ENGINEERING SCIENCE**

**FACULTY OF ENGINEERING**
**UNIVERSITY OF MALAYA**
**KUALA LUMPUR**

**2011**

# UNIVERSITY OF MALAYA

ORIGINAL LITERARY WORK DECLARATION

Name of Candidate: HIDAYAH BINTI MOHD KHALID
I.C. No.:
Matric No.: KGA080030

Name of Degree: MASTER OF ENGINEERING SCIENCE

Title of Dissertation ("this Work"):

EMBEDMENT OF HYDROXYAPATITE (HA) ON TITANIUM ALLOY (Ti6Al4V) FOR MEDICAL IMPLANT APPLICATIONS

Field of Study: ADVANCED MATERIALS

I do solemnly and sincerely declare that:

(1) I am the sole author/write of this Work;
(2) This Work is original;
(3) Any use of any work in which copyright exists was done by way of fair dealing and for permitted purposes and any excerpt or extract from, of reference to or reproduction of any copyright work has been disclosed expressly and sufficiently and the title of the Work and its authorship have been acknowledged in this Work;
(4) I do not have any actual knowledge nor ought I reasonably to know that the making of this work constitutes an infringement of any copyright work;
(5) I hereby assign all and every rights in the copyright to this Work to the University of Malaya ("UM"), who henceforth shall be owner of the copyright in this work prohibited without the written consent of UM having been first had and obtained;
(6) I am fully aware that if in the course of making this Work I have infringed any copyright whether intentionally or otherwise, I may be subject to legal action or any other action as may be determined by UM.

Candidate's Signature Date

Subscribed and solemnly declared before,

Witness's Signature Date

Name:

Designation:

# ABSTRACT

Nowadays, many researchers focus on the development of new biomaterials, which combine the osteoconductive characteristics of bioactive ceramics with sufficient strength and toughness for medical implant applications. Therefore, new coating methods have attracted great interests in recent years for replacing the high temperature techniques like plasma spraying. In this research, embedment of HA-2 wt.% Ti composite powder on superplastic and as-received Ti-6Al-4V is conducted through continuous pressing technique to improve the low strength of the conventional pure HA coatings. The embedment process is carried out at temperature below the allographic temperature in Argon gas atmosphere. The characteristics and bonding strength of the embedded layer are investigated. The bond strength evaluation is performed using wear test method under different applied pressure. HA embedded layer on superplastic and as-received Ti-6Al-4V are used for comparison. The experimental results indicated that the HA-2 wt.% Ti composite layer has uniform thickness of 8.0±0.5 μm and well bonded to the substrate. EDX and line scanning analysis revealed that HA elements are detected at the superplastic substrate indicating embedment process is successful. The X-ray diffraction pattern showed the presence of $TiO_2$ and Ti phase on the HA-2 wt.% Ti embedded surface. The surface hardness of HA-2 wt.% Ti composite layer is lower than the pure HA layer due to the intrinsic higher hardness of HA as a ceramic material. The wear test results show that the embedded layer of superplastic Ti-6Al-4V is much stronger than the as-received Ti-6Al-4V. The results also prove that the addition of Ti improves the low strength of pure HA. Observations on the surface morphology of the embedded surface show that the surface is porous but denser at the interface area. Additionally, the HA-Ti embedded layer also shows higher cohesion strength within the layer than the HA layer.

# ABSTRAK

Dalam implan ortopedik dan gigi yang tebaru, bahan seramik bioaktif telah digunakan dengan luasnya sebagai lapisan di atas prostesis besi dan implan di sebabkan kebolehannya untuk membentuk sel tisu tulang dan sifat-sifat mekanikal yang di miliki. Oleh itu, pelbagai jenis cara yang berkesan telah di aplikasikan untuk menghasilkan besi titanium yang telah dilapisi oleh bioseramik yang mana boleh digunakan dalam masa yang panjang. Dalam pembelajaran ini. 'hydroxyapatite'(HA) telah di tanam dengan jayanya ke dalam titanium aloi (Ti6Al4V) dengan menggunakan kaedah pembentukan secara superplastik, di mana ianya telah membentuk lapisan yang mempunyai saiz nanometer. Keadaan optimum bagi penenaman secara superplastik ini diperoleh dengan pembentukan yang dilakukan pada suhu 1200K dengan kadar ketangangan $1 \times 10^{-4}\ s^{-1}$ selama 90 minit. Daripada analisis X-ray difraksi (XRD) dan tenaga X-ray yang disebar (EDX) menunjukkan bahawa kistal HA masih kekal walaupun selepas proses penanaman di lakukan, dan kuantiti titanium (Ti) telah memasuki kedalam HA dengan jelasnya yang mana menunjukkan pembentukan lapisan HA/Ti yang padat telah berlaku. Ujian kehausan sample superplastik yang dijalankan dalam keadaan larutan badan (SBF) menunjukkan bahawa kekuatan dalam lapisan HA dan kekuatan antara lapisan HA dengan substrat menunjukkan prestasi yang lebih baik berbanding sample yang bukan superplastik. Selain itu, kebolehan pembentukan sampel superplastik yang telah ditanam dengan HA telah di nilai di bawah ujian mampatan pada suhu 1200 K sebanyak 10, 20 dan 30% kadar ubah bentuk. Ketebalan lapisan HA menurun daripada 249 nm kepada 240, 223 dan 206 nm dengan peningkatan kadar ubah bentuk. Melalui ujikaji morfologi sampel pada pembesaran yang besar menunjukkan retakan yang halus dan delaminasi HA telah di kenal pasti di beberapa kawasan dengan peningkatan kadar ubah bentuk. Walaubagaimanapun, pada

pembesaran yang kecil, permukaan sampel menunjukan morfologi yang lebih kurang sama untuk semua keadaan. Kekerasan permukaan menurun dari 661 HV ke 631, 604 dan 589 HV. Struktur Kristal HA masih dapat dikenalpasti walaupun selepas ujian ubah bentuk di jalankan. Daripada keseluruhan keputusan ujikaji, ia dapat disimpulkan bahawa, penanaman HA secara superplastik dapat melekat dengan kuatnya pada permukaan substrat walaupun selepas ujian ubah bentuk dijalankan tanpa merosakkan struktur HA.

# ACKNOWLEDGEMENT

All Praise be to Allah S.W.T for granting me the knowledge, health, patience and perseverance which enabled me to complete this dissertation.

My sincere gratitude goes to my supervisor, Dr. Iswadi bin Jauhari, for his persistent guidance, advice, help, and support which leads to the successful completion of this thesis. Special thanks to my supervisors at Nagaoka University of Technology (NUT), Japan, Prof. Yoshiharu Mutoh, Asst. Prof Yukio Miyashita, and Asst. Prof. Yuichi Otsuka, for granting me the opportunity to gain invaluable experience, as well as for sharing their knowledge and guidance during my UM-NUT twinning program.

My warmest appreciation goes to Mr. Nazarul Zaman of FESEM lab, Mr. Abdul Aziz f Material Science lab, and Mr. Zaini of Workshop for their technical assistance in this this dissertation.

My deepest gratitude goes to my family, especially my parents, Mohd Khalid bin A. Manap and Misnah bintin Tokimin, for their endless prayers and support in my study. I am also indebted to my beloved siblings, for their love and moral support.

My heartfelt thanks to all my friends, for their moral support and encouragement in the “thick and thin”. I am also grateful to all the unnamed people, who have directly or indirectly helped me in completing my research.

Last but not least, I would like to express my appreciation to UM for financing my research project. Under the PPP Fund (Project No. PS084-2009B) I am also indebted to UM for granting me the scholarship scheme.

# TABLE OF CONTENTS

# LIST OF FIGURES

# LIST OF TABLES

# LIST OF SYMBOLS AND ABBREVIATIONS

| Symbols | Explanation |
|---|---|
| $m$ | Strain-rate sensitivity |
| $\sigma$ | Plastic flow stress |
| $\acute{\varepsilon}$ | Strain rate |
| $K$ | Constant |

| Abbreviations | Explanation |
|---|---|
| Ti | Titanium |
| HA | Hydroxyapatite |
| Ti6Al4V | Titanium alloy |
| HBSS | Hank's balanced salt solution |
| FESEM | Field Emission Scanning Electron Microscopy |
| EDX | Energy Dispersive X-ray |
| XRD | X-ray Diffractometer |
| GBS | Grain boundary sliding |
| SPF | Superplastic forming |
| SPF-DB | Superplastic forming diffusion bonding |
| hcp | Hexagonal close packed |
| bcc | Body centred cubic |
| CP | Commercial pure |
| TMP | Thermo-mechanical processing |
| HCL | Hydrocloric acid |
| HF | Hydrofluoric acid |
| $HNO_3$ | |
| SBF | Simulated body fluid |
| Ca | Calcium |
| P | Phosphorus |
| FE | Field emission |
| S1 | Sample embedment under strain rate $6 \times 10^{-5}\ s^{-1}$ |
| S2 | Sample embedment under strain rate $8 \times 10^{-5}\ s^{-1}$ |

| | |
|---|---|
| S3 | Sample embedment under strain rate $1 \times 10^{-4}\ s^{-1}$ |
| $TiO_2$ | Titanium oxide |

# CHAPTER 1

# INTRODUCTION

## 1.1 Background

Orthopaedic and denture applications have increased significantly recently due to osteoporosis, bone damage from car and sport accidents, cancer, as well as the needs of dental/facial reconstructions (Tian and Fullbright, 2008). Therefore, artificial hard tissue replacement implant should be well integrated into the orbital muscular system without causing fibrosis of the spatted orbital connective tissues which comprise the system (Wang et al., 1996).

Titanium (Ti) and some of its alloys are commonplace for load-bearing orthopaedic implants due to their superb bio-compatibility, corrosion resistance and interesting specific mass compared with other high-strength alloys such as steels (Balazic et al., 2007; Peters et al., 2003; Tian and Fullbright., 2008; Wang, 1996; Wang et al., 1996; Watari et al., 2004). In addition, these metals are attractive for medical applications due to their ability to form apatite spontaneously on the metal surface in living organisms. Unfortunately, their applications are limited due to their low surface hardness, poor wear resistance and ineffective osteointegration with the host tissue (Kurzweg et al., 1998; Liang et al., 2004; Song et al., 2004).

Hydroxyapatite (HA) bioceramic is a truly bone-bonding material which has been applied in numerous prosthetic applications due to its osteoconductive properties and ability to bond chemically to living bone (Kurzweg et al., 1998; Thomas et al., 1980; Wang et al., 1996; Watari et al., 2004). Although beneficial, HA possesses disadvantages such that its bending strength and fracture toughness are inferior to that

of human bones. Hence, HA can be used only for applications where no important stress needs to be borne (Nonami et al., 1998; Thomas et al., 1980; Wang et al., 1996). Attempts to overcome these disadvantages have been made by using HA as a surface coating on bio-inert metallic substrates such as titanium, Ti6Al4V, and stainless steel 3I6L, whereas an alternative solution is to develop a composite composed of Ti powder and HA. The coating has been applied extensively for metallic prostheses with the aim of improving bone apposition, implant fixation and to reduce healing time (Adibah et al., 2010; Bigi et al., 2010; Chen et al. 1997; Kaya, 2008; Nonami et al., 1998).

Numerous surface coating techniques have been established to deposit HA-based coatings. These methods range from the conventional press-and-sinter method to more elegant approaches such as sputtering, electrophoretic deposition, laser deposition and plasma spraying. Among these, plasma spraying is commonly preferred because of its versatility, ability to attain fixation coating and it is economically feasible (Bigi et al., 2010; Chen et al., 1997; Kaya, 2008; Liang et al., 2004). Regardless of the coating methodology, separation or loss of HA coating is progressive with time *in vivo*, which may cause cell-mediated osteolysis and subsequent implant loosening (Bloebaum et al., 1994). Clinical reports on a patient having chronic pain and inflammation around his distal implant further emphasized the criticality of having strong coating (Taylor et al., 1996). Although the main reason for degradation of the implant was not elaborated, it is suspected that fatigue effects through chewing activities could be one of the main reasons for it. A study suggested that a HA coating thickness of 60 to 120 μm would be a better choice for clinical applications of dental implant. However, a previous study on the wear properties of HA embedded on Ti alloy demonstrated that the thicker the HA embedded layer, the easier the layer would be detached (Adibah et al., 2010). Another study indicated that thin HA coatings (~2 μm) possess significantly greater coating-

metal interfacial strength compared with commercially available thick (~70 μm) plasma-sprayed HA coatings (40 MPa vs. 9 MPa) (Rabiei et al., 2006). Moreover, the nanometre-thickness of CaP-based coatings induces an osteogenic response in vitro (De Jonge et al., 2010).

Consequently, it is deemed important to produce nanometre-thickness HA coatings in order to provide good adherence to tissue without compromising the osteogenic potential of the coatings. In this study, a new method is proposed for embedding HA onto Ti alloy using superplastic deformation approach, with the objective of producing a nanometre HA layer having a sound interlayer strength. The HA embedded layer is tested for wear under Hank's balanced salt solution (HBSS) in order to investigate the strength and stability of the HA layer under a simulated physiological condition. In addition, the feasibility of deforming the Ti embedded with HA for actual applications is revealed by high temperature compression testing.

## 1.2 Research Objectives

The objectives of this research are:

1. To propose superplastic deformation method in embedment of HA onto Ti6Al4V.

2. To evaluate the mechanical strength of Ti6Al4V superplastically embedded with HA.

3. To investigate the feasibility of forming Ti6Al4V superplastically embedded with HA in actual applications.

## 1.3 Layout of Dissertation

This dissertation is outlined as follows:

(1) Introduction

A brief background of the research, the research objectives as well as layout of the thesis is presented in Chapter 1.

(2) Literature review

The theories and concepts pertaining to superplasticity, implant coating and mechanical behaviour of coating materials were reviewed from journals, Internet websites, dissertations, theses and reference books. A summary of the literature is presented in Chapter2.

(3) Experimental procedure

The experimental procedure for superplastic embedment of Ti-6Al-4V with HA is presented in Chapter 3.The microstructures, embedded coating thicknesses and morphologies of the embedded surfaces were imaged by Field Emission Scanning Electron Microscopy (Zeiss FESEM). The distribution of Ca, P and Ti elements of the embedded surfaces and cross-section of the samples were identified by Energy Dispersive X-ray analysis (EDX) and EDX line analysis, respectively. Phase identification of the embedded surfaces was carried out using Bruker D8 Advance X-ray diffractometer (XRD). The hardness of the HA embedded surfaces was measured using Vickers microhardness tester Mitutoyo MK-17. The adherent strength of HA and interfacial strength between the HA layer and substrate in simulated physiological conditions were tested for wear under Hank's balanced salt solution (HBSS). The feasibility of Ti embedded

with HA in actual application was also evaluated in high temperature compression tests. The characterization techniques are described in Chapter 3.

(4) Results and discussion

The data, results and discussions from characterization techniques are compiled and documented in Chapter 4.

(5) Conclusions and recommendations

Conclusions of the current study and recommendations for future works are presented in Chapter 5.

# CHAPTER 2

# LITERATURE REVIEW

## 2.1 Superplasticity

Superplasticity is the capability displayed by some solid crystalline materials which have an extreme tensile deformation prior to failure. It only occurs within a narrow range of temperatures and strain rates with an optimum value which is unique to each material (Ghosh and Hamilton, 1979). Superplasticity has several different variations in terms of microstructural mechanisms and deformation conditions. There are two main types of superplastic behaviour, namely: (i) micrograin superplasticity and (ii) transformation superplasticity. Micrograin superplasticity can be recognized as fine-grained or structural superplasticity whereas transformation superplasticity is known as a deformation mechanism which occurs during the phase transformation of an externally stressed material. Examples of superplastic materials are some fine-grained metals (bismuth-tin, zinc-aluminum, titanium and aluminum) and ceramics (monoliths and composites) (Joshi, 2002).

Superplastic materials can achieve ten times or more compared with normal deformation. For deformation in a uni-axial tension, elongations to failure in excess of 200% are usually indicative of superplasticity, although several materials can attain extensions greater than 1000%. It was reported that the current world record for superplastic ductility is over 9000%, which is observed in titanium alloys (Ti-6Al-4V) through protium treatment by, as shown in Figure 2.1 (Yoshimura and Nakahigashi, 2002).

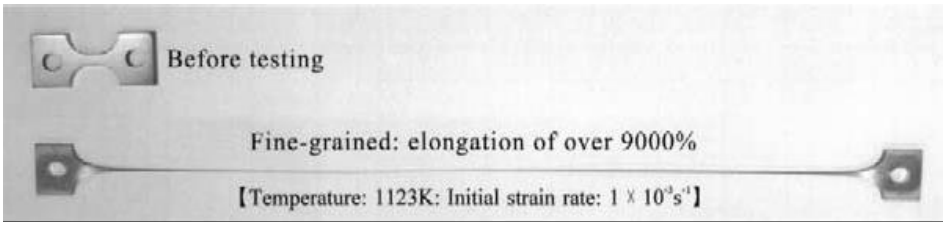


Figure 2.1: Appearance of superplastic elongated specimen of fine-grained materials (Yoshimura and Nakahigashi, 2002)

### 2.1.1 Historical Background of Superplasticity

The word superplasticity is derived from Latin and Greek words, whereby the prefix *super* means excess and *plastikos* means to give form, respectively. In 1945, Bochvar and Sviderskaya coined the term "superplasticity" to describe the extended ductility observed in Zn-Al alloys (Pilling and Ridley, 1989). Miguel Lagos also explained the theory of superplasticity using data of several alloys under a wide range of conditions. The physicist proposed that the movement of atomic vacancies creates "rolling action" which allows microcrystals to slide past one another as the material stretches.

Nowadays, many researchers have understood several aspects of superplasticity, but not at the most microscopic level. Pilling reported that the phenomenon of superplasticity can be accepted as a rubber bag filled with ball bearings, with some molasses in between. The ball bearings are grains of crystalline material less than 10 µm across. The ball bearings stay intact while the material is stretched, but they move about to accommodate a longer, thinner rubber bag. When the bag is one ball-bearing thickness, it can stretch no more (Brown, 2002).

Superplastic behaviour initially observed in the late 1920s, with a maximum of 361% for Cd-Zn eutectic at 20°C and a strain rate of ~$10^{-8}$/s and 405% at 120°C and a

strain rate of~$10^{-6}$/s. In 1934, Pearson observed a tensile elongation of 1950% without failure for a Bi-Sn alloy while working on eutectics, in which examination of bulging characteristics of the materials was performed using internally pressurized tubular specimens (Pilling and Ridley, 1989).

### 2.1.2 Characteristics of Superplasticity

Only a limited number of commercial alloys are superplastic, and these are formed via methods and conditions which are different from those for conventional metals. The basic requirements for superplasticity are: (i) very fine and stable grain size (usually less than 10μm), (ii) a temperature above about half the absolute melting temperature of the alloy and (iii) a controlled strain rate (within the strain rate range $10^{-5}$ to $10^{-1}$ $s^{-1}$) (Giuliano, 2008; Pilling and Ridley, 1989). Superplasticity is usually observed in alloys and not in pure metals. This is due to the required fine and stable grain size achieved in two-phase alloys or alloys containing fine particles which inhibit grain coarsening.

It is well known that the mechanical characteristics of superplastic materials are strongly dependent on their strain rate sensitivity of flow stress which can be defined by the Backofen equation as follows:

$$\sigma = K\acute{\varepsilon}^{m} \qquad (2.1)$$

where σ is the flow stress, ἑ the strain rate *m* the strain-rate sensitivity exponent and K is a material-related constant (Wang and Fu, 2007).

For superplastic behaviour, *m* value would be excess in about 0.3 and less than1.0. However for most superplastic materials, *m* lies the range 0.4 to 0.8 (internet reference). This indicates that *m* is a very important parameter in superplastic forming and also represents the resistance to necking in testing. Generally, the greater the *m* value, the better the resistance to necking and the better the superplasticity. Since *m* is

dependent on strain rate, the maximum *m* value has a corresponding strain rate, which is the optimal strain rate from the superplasticity deformation perspective.

The presence of a neck in a material subject to tensile straining leads to a locally high strain rate and for a high value of *m*, to a sharp increase in the flow stress within the necked region. Hence, the neck undergoes strain rate hardening which inhibits its further development. Thus, high strain rate sensitivity confers a high resistance to neck development and results in high tensile elongations characteristic of superplastic materials (Pilling and Ridley, 1989).

### 2.1.3 Mechanism of Superplasticity

A unique feature of superplastic materials is its mechanism, which is grain movement during deformation. In principle, superplasticity mechanism is similar to classical creeps of metals. These include grain boundary sliding (GBS), dislocation movement, dynamic recovery and recrystallisation process. The deformation mechanism of superplasticity is displayed in Figure 2.2.

Upon application of a small load, the motion of individual grains or clusters of grains relative to each other accumulate strain by sliding or rolling. Grains are observed to change their neighbours and to emerge at the free surface from the interior. This shows that a group of grains with a favourable orientation moves as a block relative to its neighbours. The stress concentration in the grain in which the slip plane exists and acts as a slip barrier, produces new dislocations which once again cause a slip through the grain, stopping at the next grain boundary and leading to a dislocation pile-up. The stress rise then causes slip to initiate and proceed through the blocking grain and mobility of dislocations increases by the mechanism of climb.

If grain boundary sliding is to occur in a completely rigid system of the grains, then a grain from the neighbourhood is inserted between the individual grains, as shown in Figure 2.3. Therefore, grain boundary slip is a result of the diffusion controlled mass transport along the grain boundary or through the volume of the grain (Pilling and Ridley, 1989; Siegert and Werle, 1994).

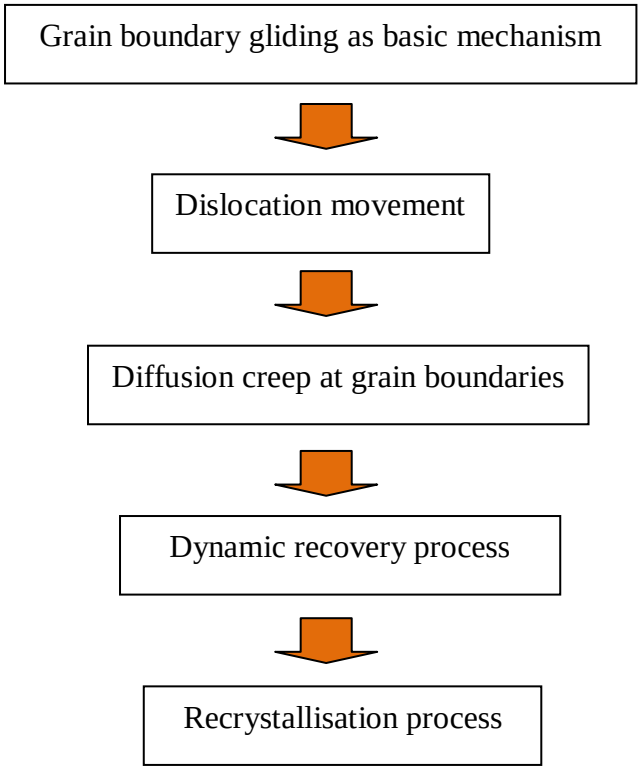


Figure 2.2: Flow mechanism of superplasticity

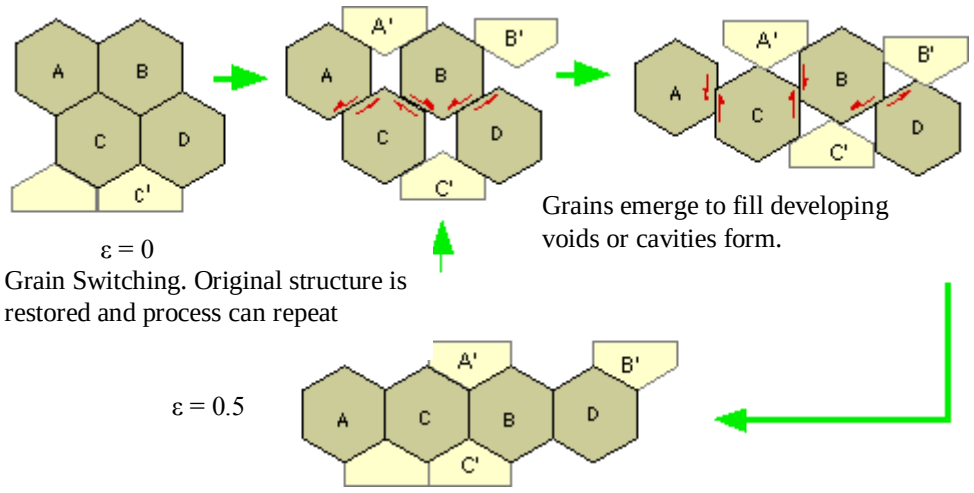


Figure 2.3: Grain movement of superplastic materials (Pilling and Ridley, 1989)

### 2.1.4 Application of Superplasticity

Nowadays, engineers use superplastics to build metal parts. Since superplasticity enables the formation of complex geometries which require extremely high degrees of ductility with minimal internal stress. Most commercial applications of superplastics are restricted to aluminium and titanium alloys which have been used to form components in aircraft and automotive industries (Ghosh and Hamilton, 1979). Normally, superplasticity is applied in two material processes, which are superplastic forming (SPF) and superplastic forming-diffusion bonding (SPF-DB).

SPF is a process which allows the formation of unique, complex shapes as well as the fabrication of components from a single piece of material (Joshi, 2002). This process can be used to produce parts which are impossible to form using conventional techniques. Once a state of superplasticity is reached, pressure is applied to the metals to allow for complex form. For this reason, SBF has been widely used in many industries which include bio-medical, aerospace, automotive and electronics. In the SPF process, *m* value is a critical parameter which represents the superplasticity of the material. Wang and Fu (2007) realised that there are three critical issues which need to

be addressed in SPF process. They are dynamic measurements of deformation velocity and loading, calculation of the *m* value, and the simultaneous control of deformation velocity (Wang and Fu, 2007). Figure 2.4 shows the SPF process in actual applications.

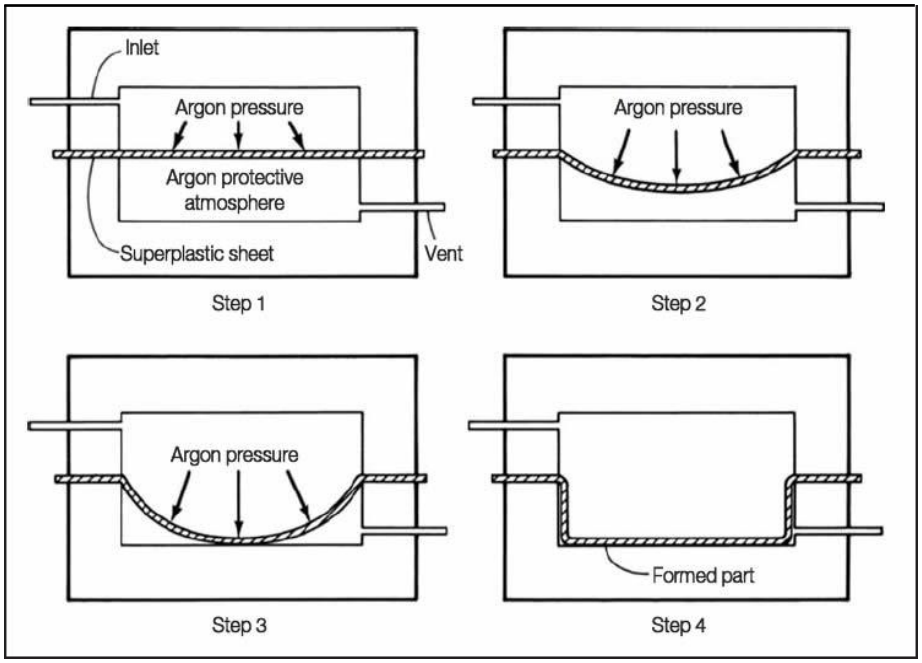


Figure 2.4: The SPF process (Madusanka, 2009)

SPF-DB is another process which combines the benefits of SPF and DB processes. DB involves atomic or elemental movement from one metal to another when two components are in contact with certain temperatures and time to remove asperities from the interface by vacancy diffusion. Concurrent forming or bonding process can save energy and reduce manufacturing costs since the method combines the benefits of each process as well as producing components with greater structural integrity and properties. Previous studies found that through SPF-DB, the advantages of two unusual properties of titanium alloys (superplasticity and diffusion bondability) results in

significant cost and weight savings compared with conventional titanium manufacturing methods (Kim et al., 2001; Lee et al., 2001; Nieh and Wadsworth, 1997).

## 2.2 Titanium and Titanium Alloy

Titanium is a white metal, and has the best strength to weight ratio among metals. It is very reactive and therefore it is often used for alloying and deoxidizing other metals (Henkel and Pense, 2001). Titanium is broadly used in a number of fields, which include aerospace, power generation, automotive, chemical and petrochemical, sporting goods and dental (Rack and Qazi, 2006; Sibum, 2003; Wang,1996). The large variety of applications is due to its desirable properties, in particular, its relative high strength, low density and enhanced corrosion resistance (Niinomi,2002). Table 2.1 illustrates the typical mechanical, physical and thermal properties of titanium (Internet Reference).

Table 2.1: Typical mechanical, physical and thermal properties of titanium

| **Property** | **Typical value** |
|---|---|
| Density | 4510 kg/$m^3$ |
| Melting Point | 1668 °C |
| Elastic Modulus | 100-120 GPa |
| Poisson's Ratio | 0.33 |
| Tensile Strength | 234 MPa |
| Yield Strength | 138 MPa |
| Percent Elongation | 54% |
| Thermal Expansion Coefficient | (8-10) × $10^{-6}$/K |

(Efunda, 2002)

Titanium is rather difficult to fabricate because of its susceptibility to oxygen, nitrogen, and hydrogen impurities, which cause titanium to become more brittle. Elevated temperature processing must be used under special conditions in order to avoid

diffusion of these gasses into the titanium. Commercially produced titanium products are made in the following mill wrought forms: plate, tubing, sheet, wire, extrusions, and forgings. Titanium can also be cast, which must be carried out in a vacuum furnace due to titanium's reactive nature (Henkel and Pense, 2001).

To overcome such restrictions, commercial pure titanium is substituted with titanium alloy. The alloying behaviour of titanium is readily discussed in terms of the effect of different solutes on the allotropic transformation temperature of the pure metal. An allotropic transformation occurs at 882°C. Below this temperature, hexagonal-close-packed (hcp) crystal structure which is known as α phase is exhibited, where body-centered-cubic (bcc) structure would be formed as a β phase at higher temperature.

The possible alloying additions stabilize one or the other of these forms, thereby raising or lowering the β transus temperature. The elements which stabilize the low-temperature form are termed α-stabilizer and those which stabilize the high-temperature form are termed β-stabilizer (Peters et al., 2003). Table 2.2 shows the effect of several elements.

Table 2.2 Alloying elements and their effects on structure

| **Alloying Element** | **Effect** |
|---|---|
| Aluminum | α stabilizer |
| Tin | α stabilizer |
| Vanadium | β stabilizer |
| Molybdenum | β stabilizer |
| Chromium | β stabilizer |
| Zirconium | α and β strengtheners |

(Gallagher, 2004)

### 2.2.1 Classification of Titanium Alloys

The control of α and β phase through alloying addition and thermo-mechanical processing is the basis for the titanium alloys used in industries nowadays. It is also a primary method for classification of titanium alloys. Titanium alloys can be categorized into three types, namely: alpha, beta, or alpha-beta, which is a mixture of the two structures. The partial phase diagram of titanium with β-stabiliser elements is depicted in Figure 2.5.

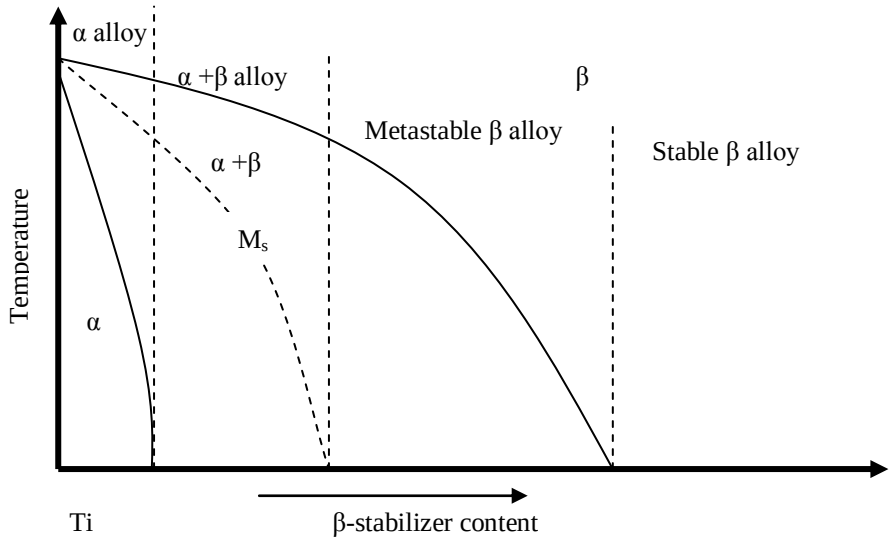


Figure 2.5: Partial phase diagram of titanium and a β-stabiliser element (Lutjeng and Williams, 2003; Long and Rack, 1998)

#### 2.2.1.1 Alpha Alloys

Alpha titanium alloys are formed by commercial pure (CP) titanium and alloys with α-stabiliser elements, whereby only the α phase is present at room temperature. These alloys typically contain aluminum and tin, although such alloys can also contain molybdenum, zirconium, nitrogen, vanadium, columbium, tantalum, and silicon. In commercially pure grades, the “normal alpha” alloy grade based on aluminum content

is known as the Ti-5%Al-2.5%Sn composition. The most extensively used super-alpha compositions are Ti-8%Al-1%Mo-1%V and Ti-6%Al-2%Sn-4%Zr-2%Mo (Si). These alloys possess the highest strength and oxidation resistance at elevated temperatures (300-600 °C) and they also have the best weldability of the titanium grades. However, these alloys have the lowest room temperature strength and are not heat treatable. This is due to the fact that no metastable phase remains after cooling from high temperature, and therefore no major modification in term of microstructure and mechanical properties are possible using heat treatment. Therefore, as α phase is not subjected to ductile-brittle transition, these alloys are proper for very low temperature application (Balazic et al., 2007; Broadwell, 2006).

### 2.2.1.2 Alpha-Beta Alloys

α + β alloys include alloys with edequate α and β-stabilisers to expand the α + β field at room temperature. Since the alloys have two phases, the compositions of the alloys vary widely. At one end of the range are the highly beta-stabilized, deep hardenable alloys such as Ti-6%Al-2%Sn-4%Zr-6%Mo and Ti-6%Al-6%V-2%Sn. These alloys provide high strengths at room and moderately elevated temperatures. At the other end of the range are the lean beta compositions, such as Ti-6%Al-4%V. They are considered to be shallow hardening, but their relatively high aluminum content results in desirable strength properties at room and elevated temperatures. The combination of α and β phase allows one to obtain optimum balance properties and the characteristics of both α and β phases may be tailored through proper heat treatments and thermo-mechanical processing. The strengths are improved after the heat treatment and higher than alpha alloys, but are less formable. Fusion weld strength efficiencies up

to 100% are attainable in alpha-beta alloys. This class makes up 60-70% of all titanium alloys used today (Broadwell, 2006).

### 2.2.1.3 Beta Alloys

Beta titanium alloys are obtained when a high amount of β-stabiliser elements are added to titanium, which decreases the temperature of the allotropic transformation (α/β transition) of titanium (Froes and Bomberger, 2005). It can be subdivided into stable beta alloys, metastable beta alloys, and beta-rich alpha+beta alloys. The first beta alloy in commercial production was Ti-13%V-11%Cr-3%Al, which is metastable. The 13% vanadium and 11% chromium additions decrease the transformation rate sufficiently for the alloy to remain 100% beta even after slow cooling. This type of titanium alloy may be hardened by using heat treatment procedures (Karasevskaya et al., 2003). It is shown by the alloys can be readily formed in the solution-annealed condition by bending at room and slightly higher temperatures and they have better weldability than alpha-beta alloys. These alloys have some advantages compared to other groups. For example, they have the highest strength of any alloying system after fully-aging. They also have the highest fatigue strength of any group of titanium alloys as a result of the high strength and fine precipitated alpha grain structure. They also have the widest range of processing possibilities after beta solution treatment which can be very soft for working and become very strong after aging.

## 2.3 Ti6Al4V Alloys

In the 1950s, Ti6Al4V was the first α + β titanium alloy developed. Although it is not the best at any particular property, it has a good combination of properties,

namely strength and workability. This alloy also has lower costs due to its larger production (Efunda, 2002).

Ti6Al4V means that the titanium has a composition of 6 wt% aluminium 4 wt% vanadium. The addition of aluminium to titanium stabilizes the α, whereas the addition of vanadium stabilizes the β phase (body-centered-cubic structure). The combination of 6% aluminium and 4% vanadium enables both allotropic modifications to exist at room temperature. Therefore, this alloy is classified as a two-phase α-β material with a β transus temperature of 995°C. The alloying additions also contribute to increased strength by solid-solution strengthening mechanisms. The complex metallurgical transformations, as well as the relative amounts of α and β phases present in the material, can affect the mechanical properties.

It is known that the mechanical behaviour of each material is directly related to composition and mainly, thermo-mechanical processing. The properties of Ti6Al4V are dependent on the heat treatment process which it previously encountered. Several mechanical properties of Ti6Al4V applicable for biomaterials are given in Table 2.3 (Bardos, 2006).

Table 2.3: Typical mechanical properties of Ti6Al4V alloys for medical applications

| **Mechanical Property** | **Value** |
|---|---|
| Ultimate tensile strength (MPa) | 965 |
| Yield strength (Mpa) | 895 |
| Young's modulus (Gpa) | 110 |
| Elongation (%) | 12 |
| Fatigue endurance limit at 107 cycles (Mpa) | 515 |

(Bardos, 2007)

Nowadays, this alloy is known as the most widely titanium alloy in industries such as surgical implant, prosthetic devices, jet engines and aircrafts. It is documented that its commercial applications are due to its superior properties such as high-strength-to-weight ratio, good fatigue life and excellent corrosion resistance (Boyer, 1996).

### 2.3.1 Pre-heat Treatment of Ti6Al4V

The mechanical properties and microstructure development of titanium and its alloys are exceedingly dependent on the processing and heat treatment that they undergo (Gallagher, 2004). The purposes of heat treatment of titanium and its alloys are to reduce residual stresses developed during fabrication, to produce an optimum combination of ductility, machinability, dimensional and structural stability and to increase strength (Henkel and Pense, 2001). Heat treatment is dependent on the cooling rate from the solution temperature and can be affected by the size of the component.

There are two basic microstructural morphologies which control the basic mechanical behaviour of these alloys, which are the lamellar transformed beta microstructure and the primary (equiaxed) alpha (Efunda, 2002). The primary α can exist in various forms elongated plates to globular sections depending on whether the material is lightly or heavily worked. The transformed β regions are those of β phase at the working temperature, which vary depending on the cooling rates.

Previous studies have shown that thermo-mechanical processing (TMP) of the (α + β) titanium alloy above the β transus temperature leads to a 'lamellar' microstructural morphology, consisting of α platelets with an inter-platelet β phase. The 'lamellar' structure varies with cooling rate, ranging from colonized platelike α at a low cooling rate, a basketweave morphology at an intermediate cooling rate, Widmanstätten at a high cooling rate, to martensite, when quenched in water. When processed below

the β transus, Ti6Al4V shows an (α + β) structure with the prior α phase retained to room temperature and the β phase transformed in part. The heat treatment process for a common titanium alloy, Ti6Al4V is shown in Figure 2.6.

In addition to processing temperature, other hot working parameters, such as strain and strain rate, also affect the microstructure, e.g. the volume fractions of the α and β phases, the phase size and the 'lamellar' dimensions of the α phase. The aspect ratio of the α lamella phase is also a very important factor which influences the mechanical properties of Ti6Al4V alloy (Froes, 1985). Previous studies showed that dynamic or metadynamic recrystallisation could occur for Ti6Al4V during isothermal forging and hot compression (Park et al., 2008).

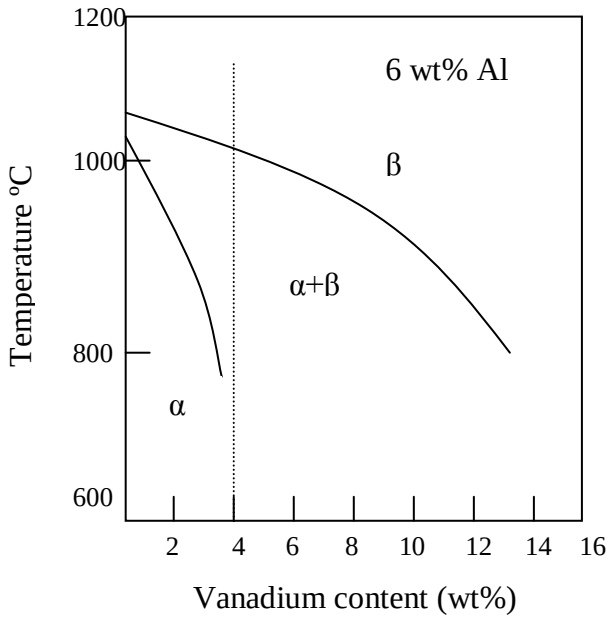


Figure 2.6: Microstructure development on Ti6Al4V ( Gallagher, 2004)

## 2.3.2 Superplastic of Ti6Al4V

One of the titanium alloys which have been extensively studied in aspect of superplasticity is Ti6Al4V alloy. It is found that, under particular conditions, this alloy exhibits superplastic properties which allow for large plastic deformation. The

formability of this material is greatly improved through superplastic forming process, resulting in weight reduction and cost savings. Accordingly, many efforts have been concentrated on the enhancement of superplasticity within the frameworks of chemical composition and grain refinement. Edington et al. reported that enhancement of superplasticity can be obtained through the most efficient methods of grain refinement (Edington et al., 1976). In this method, a stable and fine-grained Ti6Al4V alloy was formed through the conversion of the transformed beta microstructure to a fine equiaxed microstructure (dynamic globurization). It was mentioned in section 2.1.2 that a fine grain size of less than 10 μm is essential for the occurrence of GBS, which is the predominant deformation mechanism in superplastic materials. In addition, the deformation temperature has to be superior to half of the melting temperature, whereas the strain rate must be situated in the range of $10^{-4}\ s^{-1}$ and $10^{-2}\ s^{-1}$ (Chandra, 2002). More to the point, in a previous study by Ghosh and Hamilton, the Ti-6Al-4V alloy is known to be superplastic approximately between 750°C and 950°C, and at strain rates between $10^{-4}\ s^{-1}$ and $5 \times 10^{-3}\ s^{-1}$ (Ghosh and Hamiton, 1979).

## 2.4 Titanium and Titanium Alloys in Medical Applications

Titanium may be considered a relatively new engineering material. The initial commercial development of titanium in the late 1940s was soon followed by its evaluation as a surgical implant material (Balazic et al., 2007). It is known that its usage as an implant material began in the 1960s, despite the fact that titanium exhibits superior corrosion resistance and tissue acceptance compared with stainless steels and Cr-Co-based alloys (Wang, 1996). Nowadays, titanium plays a significant role in numerous surgical procedures in the field of orthopaedic, cardiovascular and dental implantation.

In terms of biomedical applications, the properties of interest are biocompatibility, corrosion behaviour, mechanical behaviour, processability and availability (Disegi, 2002). Of the many titanium alloys that have been found suitable for medical applications, it is known that Ti6Al4V is the most widely used alloy, due to its superior mechanical properties compared with other competing materials. It is documented that the yield strength is approximately the same as that of surgical quality 316L stainless steel and almost twice as that of the familiar cast Co-Cr0Mo alloy used in orthopaedic implants. The elastic modulus is approximately half of that of other common metal alloys used in surgery. The low modulus results in a material which is less rigid and deforms elastically under applied loads. These properties play a significant role in the development of orthopaedic products in which a close match is desired between the elastic properties of long bone and surgical implant.

The outstanding biocompatibility of these materials was discovered by (Bothe et al., 1940 and Leventhal, 1951) in their early animal experiments. No any cellular changes adjacent to titanium implant and no adverse clinical effects were detected through histopathological examinations. In addition, careful examination of tissue adjacent to Ti-6Al-4V alloy has revealed neither giant cells not macrophages, nor other signs of inflammation. Therefore, the material is found to be safe in intravascular applications owing to its high electronegativity and passive surface.

Despite its impressive biocompatible property in bioimplant applications, titanium and its native oxide thin film are known to be bio-inert, and the ability of its surface to induce apatite formation is rather poor (De Jonge et al., 2010; Ishikawa et al., 1997; Onoki et al., 2008). For this reason, hydroxyapatite (HA) coatings are used as bioactive surface of titanium implants, of which many surface treatment techniques have been developed. The concept of bioactive coatings uses the principle of enabling

interfacial chemical bonds between the implant and the bone tissue due to a specific biological response (Hench, 1998). Surface modifications should provide distinct properties of interaction with cell molecules, which promote the adaption or in-growth of cells or tissue onto the surface of fixation elements of a medical implant or prevent cell interactions with the implant surface.

## 2.5 Hydroxyapatite

Hydroxyapatite (HA) is a mineral which is a natural form of calcium apatite with a chemical formula of $Ca_{10}(PO_4)_6(OH)_2$ and a Ca/P molar ratio of 1.667. It is known as a good candidate for bone replacement because of its chemical similarities to the inorganic component of bone and tooth (Hench, 1998). In addition to being a very good osteoinductor for the in-growth of natural bone, it is widely used as a bioceramic in reconstructive surgery, dentistry as well as drug delivery materials (Yuan). Despite their favourable biological properties, the poor mechanical properties of HA bioceramics have severely hindered their clinical applications and limits their use as loading-bearing implants (Lin et al., 2007; Orlovski et al., 2002).

In order to overcome this drawback, HA has been applied as a surface coating on bio-inert metallic substrates, such as titanium, Ti6Al4V, and stainless steel 316L. However, in recent years, titanium and its alloys are the most commonly used materials for load-bearing orthopaedic implants mainly due to their superior biocompatibility and low density (Long and Rack, 1996; Sousa and Barbosa, 1996).

## 2.6 HA coating and embedment process

It is well documented that the integration of metallic implants with surrounding bones can be improved by the presence of biologically active calcium phosphate layer on metal implant in a living body. In order to create bioactive layer, various techniques have been used in the coating of HA bioceramics onto metallic substrates such as plasma spraying, electrophoretic deposition and sputtering (Cotell et al., 1992; Kurzweg et al., 1998). Among these, plasma spraying is known as the most often used coating process due to its versatility, ability to attain a fixation coating and the method is economically feasible (Bigi et al., 2010; Chen et al., 1997; Liang et al., 2004; Kaya, 2008). However, a plasma-sprayed HA coating gradually dissolves as a time proceeds, and is doomed to come off due to brittleness and low crystallinity, meaning an anxiety for the loosening of implants. Therefore, the establishment of a reliable method to fix HA on the implants with long-term stability after implantation is one of the keys for successful dental/orthopaedic implantation.

For dental/orthopaedic implants to achieve better apposition and bone-implant bonding, some works introduced the embedment of HA using continuous pressing method at elevated temperatures, which can be considered as superplastic deformation-like method (Adibah et al., 2020; Ramdan et al., 2008; Sanaz et al., 2010). In this method, it is expected that the diffusion process can occur from high-temperature conditions and additional pressing work provides additional energy which force bio-apatite to move inside the substrate. This, in turn, enhances the bonding properties of bio-apatite on the substrate. In addition, the surface asperities of the superplastic Ti6Al4V substrate can be easily plastically deformed through this method, which expedites the embedment between bioceramic powder and substrate.

Nonami et al. also revealed that the bone implant fixation was improved by the hot pressing method in implanting HA granules into superplastic titanium alloy substrate. This is due to the occurrence of a mutual reaction occurs between the granules and alloy and it seems that there is a chemical reaction in the interface of the granules and the titanium alloy (Nonami et al., 1998). Therefore, a preliminary study is carried out to superplastically embed HA into Ti6Al4V alloy and to investigate the adherent strength of HA and the strength between the HA layer and substrate.

# CHAPTER 3

# EXPERIMENTAL PROCEDURE

## 3.1 Materials and Specimen Preparation

### 3.1.1 Materials

Ti6Al4V (Grade 5) with an average grain size of 13 ± 0.5 μm is used as the substrate material and the chemical composition of this alloy is listed in Table 3.1. Hydroxyapatite powder with a mean diameter of 10 ± 0.5 μm is used as the embedment material and is supplied by Taihei Chemical Co. Ltd. Tokyo, Japan.

Table 3.1: Chemical composition of Ti6Al4V

| Element | Titanium, Ti | Aluminium, Al | Vanadium, V | Carbon, C |
|---|---|---|---|---|
| Wt% | 88.05 | 6.73 | 3.9 | 2.12 |

### 3.1.2 Specimen Preparation

The titanium alloy samples are machined with a dimension of 10 × 10 × 3 $mm^3$ from the as-received material using cutter and lathe machine, as shown in Figure 3.1. The lathe machine is used to make the edges of the samples smooth and flat in order to obtain a precise size.

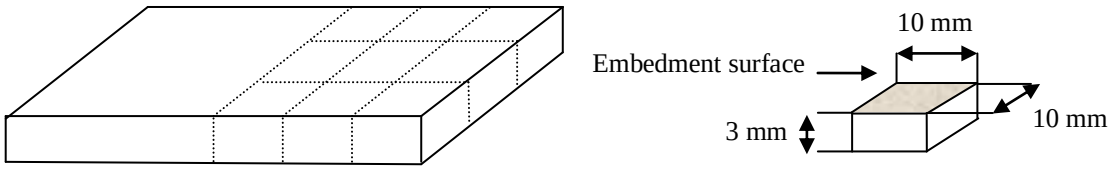


Reference: ..... Cutting point

Figure 3.1: Dimension of the sample before embedment

## 3.2 Heat Treatment

In this study, the as-received Ti-6Al-4V is heat-treated to achieve a full martensite (metastable phase) microstructure. The objective of this treatment is to obtain a suitable superplastic condition for the sample during the embedment process. The heat treatment process is shown in Figure 3.2.

To ensure thermal equilibrium and formation of fully martensite microstructure during the quenching process, the samples are hug inside the furnace heated to 1373 K (beta-transus temperature at which alpha + beta → beta: ≈ 1250 K). Once the temperature reached 1373 K, the samples are held for 30 minutes for the purpose of homogenization. Following this, the samples are ice quenched to room temperature, in which the samples are dropped immediately into the container containing ice and water (~ 273 K) which is placed under the furnace. Figure 3.3 shows the set up apparatus used for heat-treatment process.

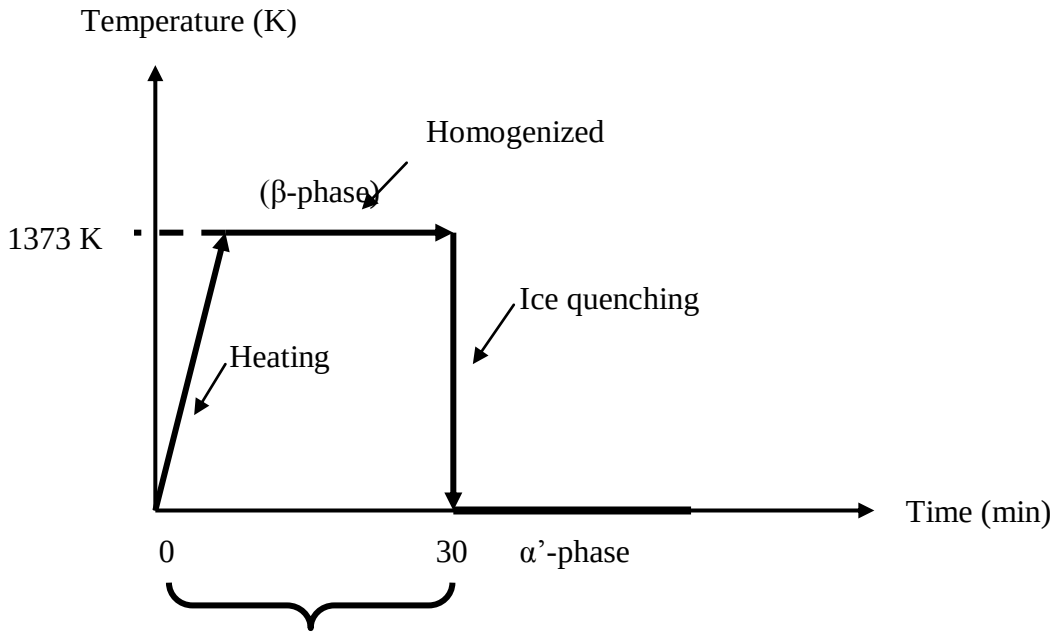


Figure 3.2: Heat treatment process on Ti6Al4V

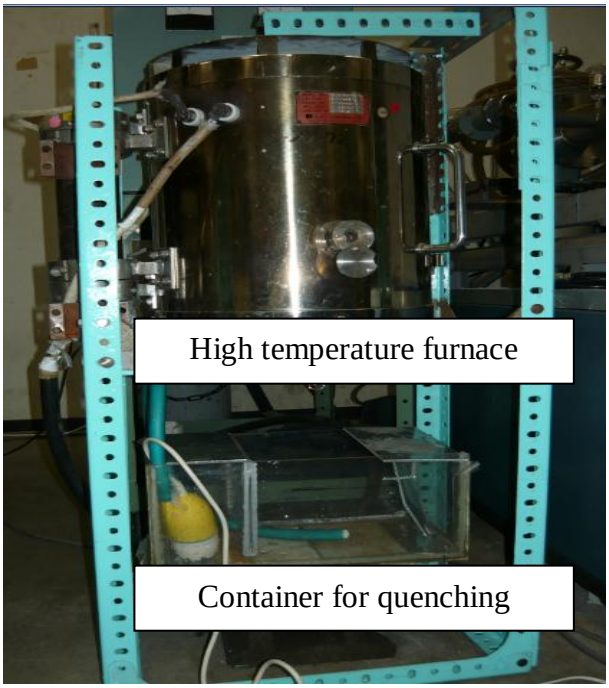


Figure 3.3 Set up apparatus used for the heat treatment process

## 3.3 Superplastic Embedment Process

In the embedment process, hydroxyapatite (HA) bioceramic is applied as an embedding material due to its chemical similarity to the inorganic component of human bone. Prior to the embedment process, the heat-treated sample surfaces are polished using emery paper with a grit size of up to 1200 and cleaned with alcohol to remove oxide layers and irregularities. The embedment process is conducted using a compression testing machine (Instron) equipped with a high-temperature furnace under a controlled gas atmosphere. Argon gas is used as the controlled gas throughout the process to prevent gas diffusion into titanium, which would cause the titanium to become more brittle. A schematic diagram of the experimental apparatus and the position of the heat-treated Ti6Al4V with 2g of hydroxyapatite powder placed inside a specially designed die are shown in Figure 3.4. In this study, a puncher which is located on the sample is used to homogenize the embedment process. This assembly is heated from room temperature to the embedment temperature (1200 K) and maintained for 1 h before being compressed under a certain strain rate until the material attains 54 % reduction in thickness. When the process is completed, the sample is cooled to room temperature in the furnace. The embedment samples prepared under different strain rates (i.e. $6 \times 10^{-5}$ $s^{-1}$, $8 \times 10^{-5}$ $s^{-1}$ and $1 \times 10^{-4}$ $s^{-1}$) are labelled S1, S2 and S3, respectively. The cross-sections of the embedded samples are ground and polished until mirror surfaces are attained. The samples are then etched using Kroll's reagent (a mixture of 3 ml HCL (36%), 2 ml HF (48%) and 5 ml $HNO_3$ (65%) in 190 ml of distilled water) for 10 s before physicochemical characterisation.

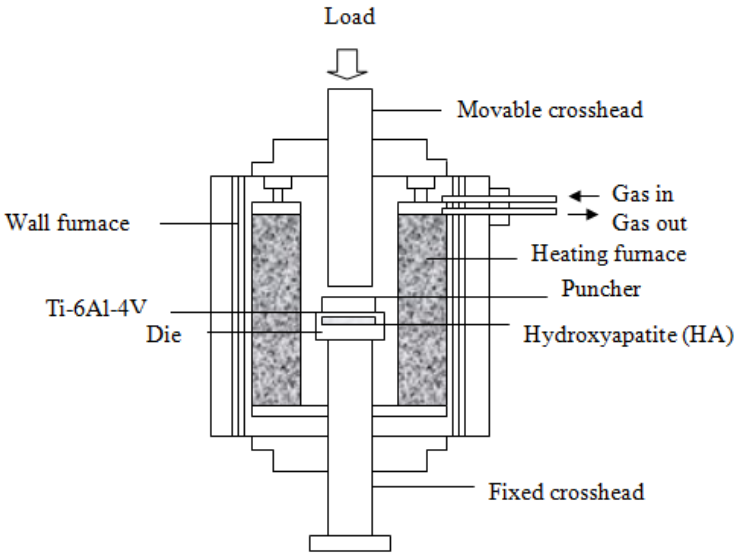


Figure 3.4: Schematic diagram of compression test

## 3.4 Mechanical Testing of HA Embedded Layer

Long-term mechanical stability is a fundamental requirement for HA coatings on metals. Critical factors such as implant surface characteristics, adhesion strength of the coating to the implant surface and in vivo and in vitro bioactivities require attention. For these reasons, two types of testing are conducted in this study after the embedment process.

### 3.4.1 Wear Test

In order to test the bonding strength of the HA layers in a biological environment, wear tests are carried out against polishing cloths under 500 ml simulated body fluid (SBF) solutions at room temperature for 30 min. Hank's balanced salt solution (HBSS) is used as the SBF in this study (Choubey et al., 2004).The tests are performed using a modified polishing machine with a rotational speed of 165 rpm. Various pressures (0.05, 0.1, 0.2 and 0.4 MPa) are applied on the samples. A schematic

diagram of the equipment used is shown in Figure 3.5. The same sample is used for each applied pressure during wear tests. After the wear tests for each applied pressure, the embedded coating thicknesses are measured, whereas the morphology and distribution of Ca, P, Ti elements for the embedded surface are evaluated for each load condition.

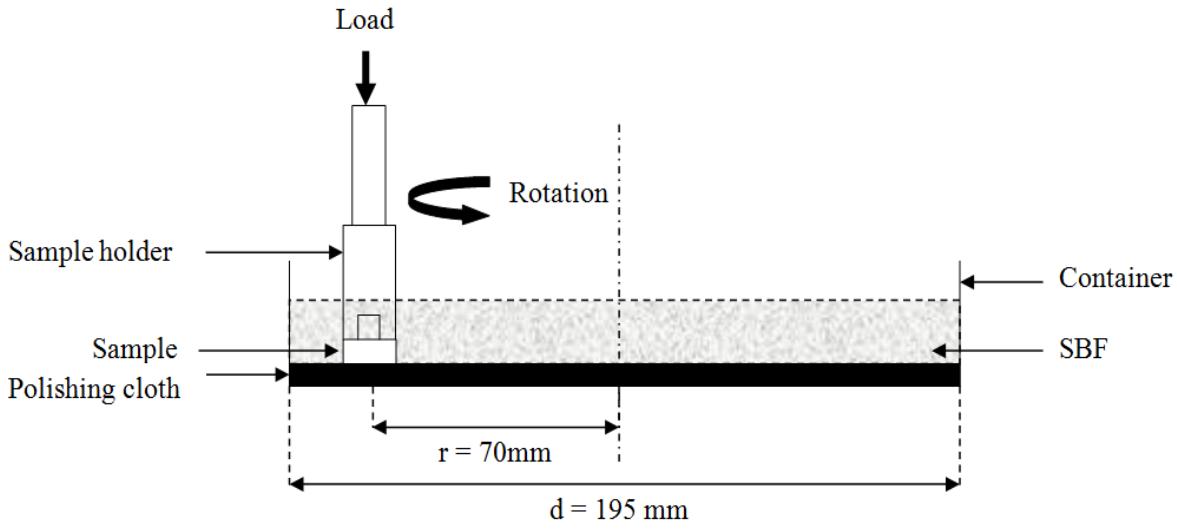


Figure 3.5: Schematic diagram of wear testing

### 3.4.2 High Temperature Compression

A vast number of complex shaped implants are urged yearly. The feasibility of forming Ti alloy superplastically embedded with HA nanolayer under compression mode is examined. The S3 embedded sample (refer section 3.3) is reheated at 1200 K, held for 1 h for homogenization and compressed at a constant strain rate of $1.6 \times 10^{-3}\ s^{-1}$ until a height reduction of 10, 20 and 30%. The compression process is conducted using a compression test machine (Instron) equipped with a high temperature furnace in Argon gas atmosphere. The argon gas is used to prevent undesirable phase formed on the HA embedded layer. Figure 3.6 shows the apparatus and position of the sample in a designed die used for the deformation process. When the process was completed, the

furnace is air cooled to room temperature. Following the deformation processes, the embedded coating thicknesses are measured and the morphologies of the embedded surfaces are evaluated for each condition.

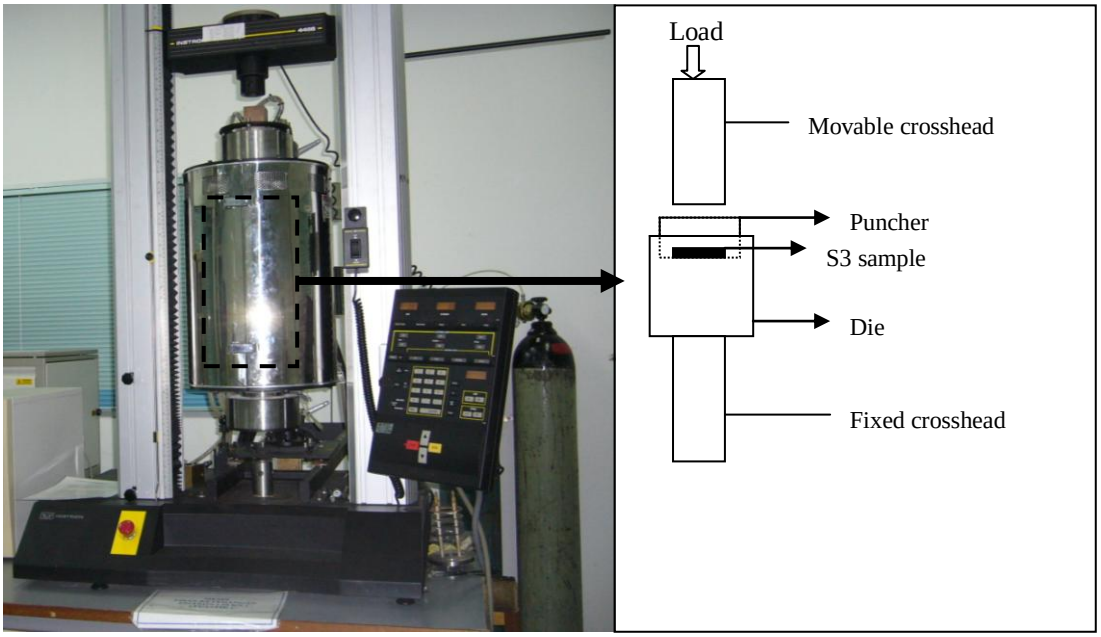


Figure 3.6: Instron machine with a schematic diagram of the compression testing

## 3.5 Characterization Methods

The microstructures of the samples, embedded coating thicknesses and morphologies of the embedded surfaces corresponding to different tests are then imaged by Field Emission Scanning Electron Microscopy (Zeiss FESEM). Phase identification of the embedded surfaces is carried out using X-ray diffractometer (XRD) and the distribution of Ca, P and Ti elements of the embedded surfaces and cross-section of the samples are identified by Energy Dispersive X-ray analysis (EDX) and EDX line analysis, respectively. Vickers hardness test is also conducted using Vickers microhardness tester to measure the hardness of the HA embedded surfaces.

### 3.5.1 X-ray Diffraction

X-ray diffraction (XRD) is a non-destructive technique used to identify the chemical compositions and crystallographic structures of natural and manufactured materials. XRD results are displayed similar as fingerprints with different patterns. The XRD pattern is formed when X-rays directed on a crystalline material may experience diffraction (constructive interface) as a result of its interaction with a series of parallel atomic planes according to Bragg's Law. In this law, the wavelength of electromagnetic radiation is related to the diffraction angle and the lattice spacing in a crystalline sample. These diffracted X-rays are then detected, processed and counted (Dutrow and Clark, 2011).

In this study, Bruker D8 Advance X-ray diffractometer (XRD) which employs Kα radiation at 40 kV and 40 mA is used to identify the type of crystal structure formed for every condition. The scanning range (2θ) is within 20˚ to 80˚ at a scan speed of 0.1˚ $sec^{-1}$ and a step size of 0.02˚. The XRD machine is shown in Figure 3.7.

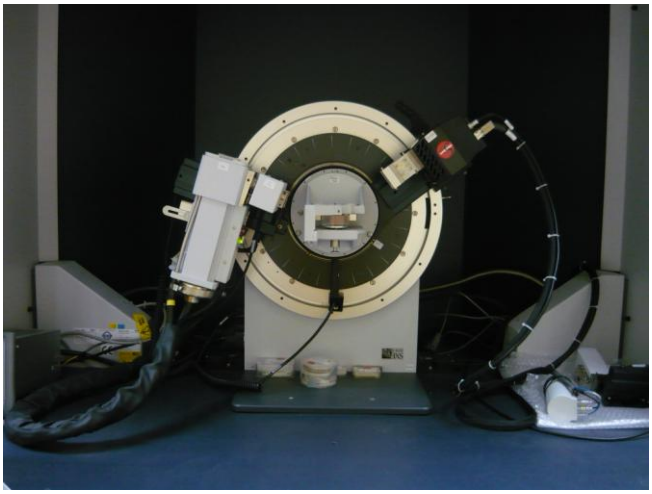

Figure 3.7: X-ray diffraction machine

### 3.5.2 Field Emission Scanning Electron Microscopy

Field emission scanning electron microscopy (FESEM) is a very useful tool for high resolution surface imaging nanomaterials science. It is a microscope that works with electrons (particles with a negative charge) which are liberated by a field emission (FE) source. The electrons are accelerated in a high electrical field gradient. Within the high vacuum column these so-called primary electrons are focused and deflected by electronic lenses to produce a narrow scan beam which bombards the object. Consequently, secondary electrons are emitted from each spot on the object. The angle and velocity of these secondary electrons relates to the surface structure of the object. A detector catches the secondary electrons and produces an electronic signal. This signal is amplified and transformed to a video scan-image that can be seen on a monitor or to a digital image that can be saved and processed further (Wikimedia Foundation Inc., 2011).

Zeiss Auriga FESEM is used in this study with maximum ×50000 and enlargement is connected by a Panasonic digital camera model WV-CP410 to an image analyzer SmartSEM V05.04 operating software. Figure 3.8 shows the FESEM machine.


Figure 3.8: FESEM machine

### 3.5.3 Energy Dispersive X-ray Spectroscopy

Energy-dispersive X-ray spectroscopy (EDX) is an analytical technique used for elemental analysis or chemical characterization of samples. EDX systems are mostly commonly found on scanning electron microscopes (SEM-EDX). In this study, the EDX system is coupled with the FESEM. There are four primary components of EDX: beam source, X-ray detector, pulse processor and the analyser (Materials Evaluation and Engineering, Inc., 2009). The EDX detector measures the relative abundance of emitted X-rays versus their energy. When an incident X-ray strikes the detector, it creates a charge pulse which is proportional to the energy of the X-ray. The charge pulse is converted to a voltage pulse by a charge-sensitive preamplifier. This information is sent to a pulse processor, which measures the signals and passes them onto an analyser for data display and analysis.

In this study, the elemental composition of HA embedded surface is identified by energy dispersive X-ray analysis (EDX) and line scanning is used with 20 kV voltage to exhibit the interdiffusion of Ti element from the HA layer to the substrate.

### 3.5.4 Microhardness Tester

Microhardness tester is an apparatus used for hardness tests, which is available as a relatively simple alternative to tensile tests. The term ‘microhardness test’ usually refers to static indentations made with loads not exceeding 10 N. The indenter is the Vickers diamond pyramid. The procedure for testing is very similar to that of standard Vickers hardness test, except that it is carried out on a microscopic scale with higher precision instruments. Precision microscopes are used to measure the indentations. Usually, a magnification is around ×500 with accurances of ± 0.5 mm (Gordon England, 2008).

In this research, Mitutuyo microhardness tester model MVK-H2 fitted with a Vickers indenter under a load of 50 kgf is used to measure the surface hardness of HA embedded layer. Figure 3.9 shows the microhardness tester. The reader would give the hardness value automatically after the size of diamond is measured.


Figure 3.9: Microhardness tester

# CHAPTER 4

# RESULTS AND DISCUSSION

## 4.1 Ti6Al4V Substrate

In this study, as-received titanium alloy (Ti6Al4V) with a grain size of around 13.0 ± 0.5 μm was used as the substrate. The microstructure of the as-received Ti6Al4V alloy is shown in Figure 4.1, which consists of an equiaxed primary α-phase with secondary (platelet) α and a small amount of intergranular β. In order to achieve the optimum processing condition for the following process (embedment process via superplastic deformation), the as-received substrates are heat treated. During heat treatment, the as-received microstructure transformed rapidly into the α' martensite phase, which consists of parallel-sided plates (lamellar) or laths, as shown in Figure 4.2.

Normally, lamellar microstructural morphology has good resistance to fatigue crack propagation as well as high fracture toughness (Gnanamoorthy et al., 1996; Shibata et al., 1996). However, Ti6Al4V alloys with this morphology are rarely produced for industrial applications due to their poor ductility. Thus, development of equiaxed recrystallised structure is required to ensure the formability of this material with a vast range of industrial applications. The equiaxed recrystallised structure can be greatly attained through grain refinement process. In this regard, many studies have reported that grain refinement is an effective method to enhance the mechanical strength without the need of adding a potentially harmful alloying element (Kim et al., 2006; Zhao et al., 2004).

It has been stated that, the formation of acicular α' martensite structure during heat treatment is beneficial for the embedment process via superplastic deformation. This is due to the fact that the meta-stable microstructure (α' martensite), has many dislocations both inside the grains and around the grain boundaries, which creates a material with high grain boundary energy. The extra internal energy hastens grain refinement, and grain boundary sliding (GBS) occurs easily when the material deforms superplastically during the embedment process.

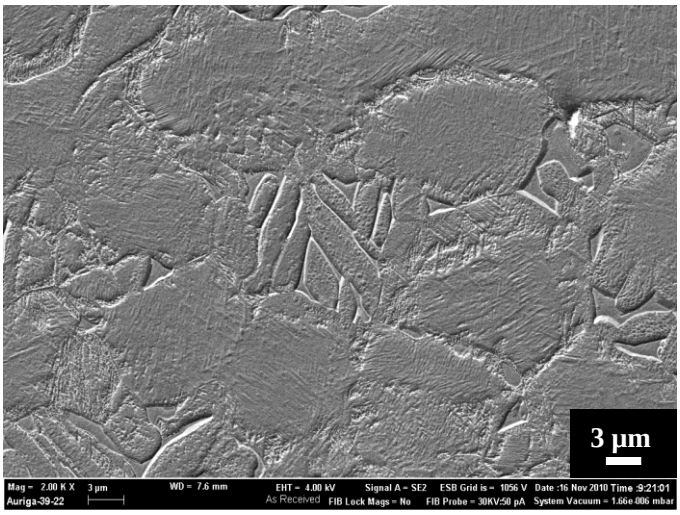


Figure 4.1: FESEM image of as-received Ti6Al4V

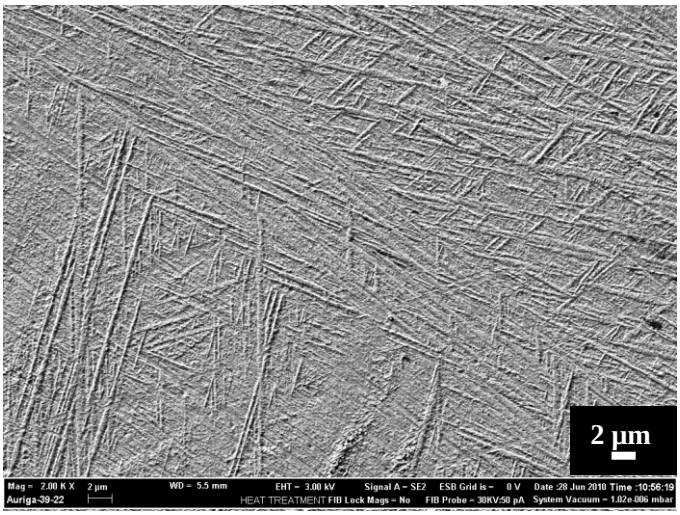


Figure 4.2: FESEM image of Ti6Al4V after heat treatment

The hardness value of the as-received and heat-treated Ti6Al4V is tabulated in Table 4.1 measurements were carried out to study the effects of the heat treatment process on the toughness of the substrates. It is found that, the hardness value of the heat-treated Ti6Al4V increases from 317 ± 0.5 HV to 478 ± 0.5 HV.

The increase in of hardness can be explained by the formation of martensite structure ($\alpha + \beta \rightarrow \alpha'$) during rapid quenching of the substrates in ice. It is known that the mechanical properties and microstructure development of titanium and its alloys are strongly dependent on the process and heat treatment. This is also one of the key reasons why titanium alloys are able to accommodate many different applications (Markovsky, 1995).

Table 4.1: Hardness of Ti6Al4V in different conditions

| **Condition** | **As-received** | **Heat-treated** |
|---|---|---|
| **Hardness (± 0.5)** | 317 | 478 |

## 4.2 Superplastic Deformation and Embedment of Hydroxyapatite (HA) onto Heat-treated Ti6Al4V Alloy

### 4.2.1 Superplastic Deformation

Superplasticity is known as a diffusion-controlled process which is greatly influenced by grain refinement (Edington et al., 1976). For this reason, in this study, the embedment of HA onto the substrate was introduced by superplastically deforming the Ti-6Al-4V alloy having a martensite microstructure under compression tests. This process is termed as "superplastic embedment". Figure 4.3 shows the stress - strain curves obtained from the deformation of substrates at different strain rates, up to a strain of 0.54. Since the tests were performed at different strain rates, the time duration spent for each embedment process was also different. From Figure 4.3, it is observed that the curve with the slowest strain rate produced the lowest maximum stress of about 80 MPa whereas the other two curves produced much higher stresses, with a value of 157 and 155 MPa, respectively. Generally, the faster the strain rate, the higher the resultant peak stresses. However, it shall be noted that although sample S3 deformed at a relatively faster rate than sample S2, S3 exhibits a lower peak stress value. Table 4.2 summarizes the deformation properties for each condition.

Figure 4.4 illustrates the appearance of the samples before and after embedment. The actual strain for each sample measured after embedment is shown in Table 4.2. S1 shows the lowest strain compared with S2 and S3, with a value of 0.17. This may be due to the fact that the applied stress during the embedment process is much lower for S1 compared with the other two samples (refer Figure 4.3). For S2 and S3, the actual strains for both samples are around 0.34. The relatively higher applied stress during embedment produces a higher amount of plastic strain.

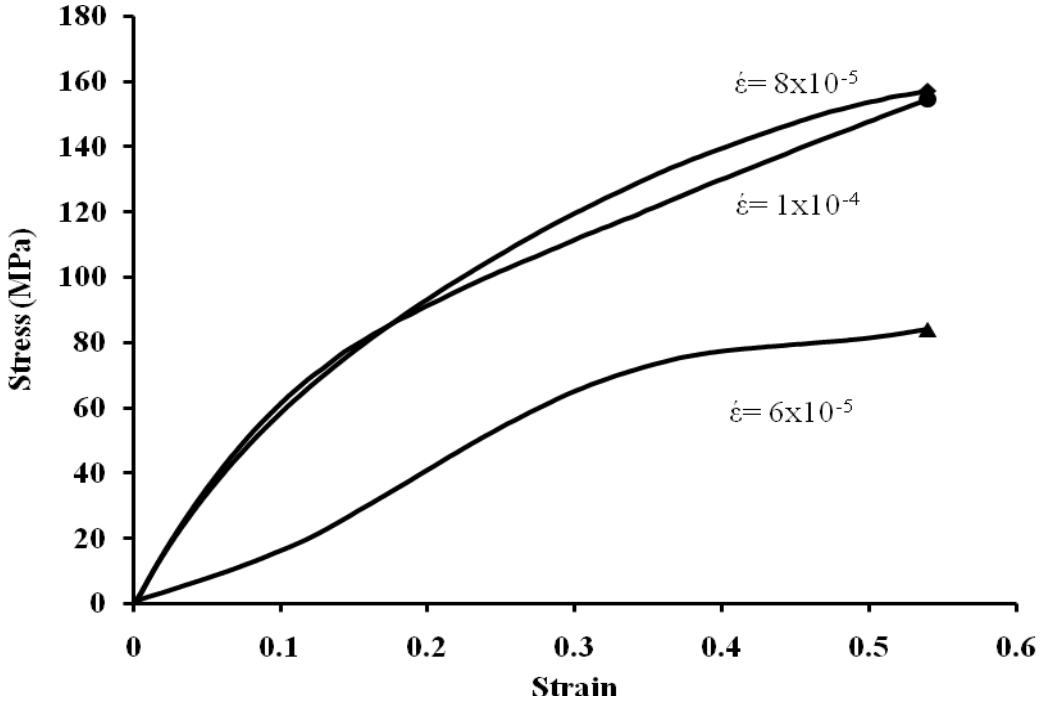


Figure 4.3: Typical stress-strain curves of Ti6Al4V alloy after embedment process under various strain rates at 1200K

Table 4.2: Deformation properties of samples compressed at different strain rates until 0.54 strain

| **Strain rate, $s^{-1}$ (Sample)** | **$6 \times 10^{-5}$ (S1)** | **$8 \times 10^{-5}$ (S2)** | **$1 \times 10^{-4}$ (S3)** |
|---|---|---|---|
| **Maximum load, MPa** | 84 | 157 | 155 |
| **Time, min** | 150 | 113 | 90 |
| **Actual strain of substrate** | 0.17 | 0.34 | 0.34 |
| **Grain size, µm** | lamellar | 3.5±0.5 | 2.6±0.5 |

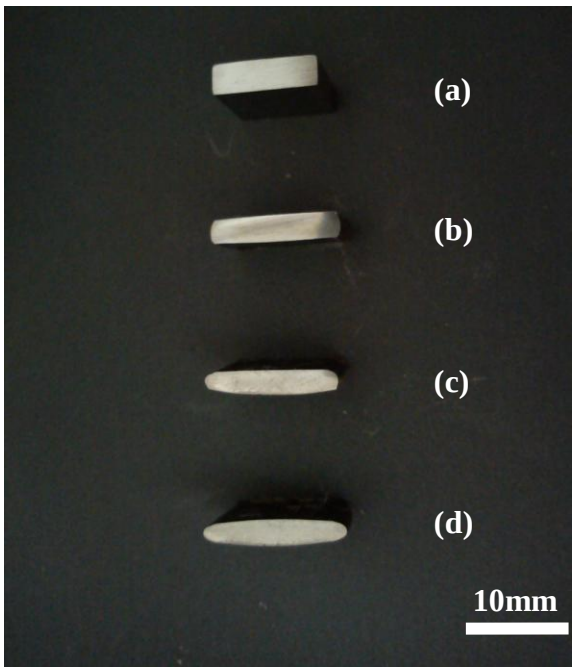


Figure 4.4: Side view of sample: (a) before embedment (b) S1, (c) S2 and (d) S3

The microstructures at most sections of the sample after deformation are depicted in Figures 4.5 – 4.7. For S1, as evidenced in the micrograph of Figure 4.5, the lamellar microstructure is still retained as well as the remnant alpha plate. The lamellar microstructure may be attributed to the break-up of the prior α lamellar during hot working (Ding et al., 2002). In addition, previous research reported that this microstructure is formed before the grain refinement stage takes place (Semiatin et al., 1999).

Figures 4.6 and 4.7 exhibit the evolution of the microstructure at higher strain rates (S2 and S3). At these strain rates, full grain refinement is observed, in the sense that fine equiaxed microstructures of β rich α+β titanium alloy appear. The average grain size for the two samples is 3.5 ± 0.5 and 2.6 ± 0.5 μm, respectively. As mentioned previously, a fine grain size of less than 10 μm is essential for the occurrence of superplastic deformation. The fine grains allow GBS, which is the main mechanism in

superplastic deformation, (Vanderhasten et al., 2005). Based on these facts and the results obtained, S2 and S3 can be considered to have achieved superplastic condition. However, from a practical aspect, if the required properties are able to be produced, a shorter process duration is desirable. In this case, S3 is more desirable than S2 because although S3 deformed at a relatively higher rate, S3 produces finer grains compared with S2. Thus, in the following sections, all discussions pertaining to superplasticity are focused solely on S3 sample.

### 4.2.2 Embedded layer properties and characterisation

The surface morphologies of the HA embedded surface for the S1 and superplastic S3 are presented in Figure 4.8 and 4.9, respectively. In this study, the HA embedded surface contains two types of morphologies: well-melted HA and unmelted HA particles. From Figure 4.8, the surface of S1 is relatively rough with a dispersion state of unmelted HA coarse particles scattering on the surface, as highlighted in white circles. A smoother surface is obtained for the superplas sample (S3), as shown in Figure 4.9. The embedded surface exhibits well-melted splats (marked by the black arrows) with a very fine globular of unmelted HA (marked by the white arrows).

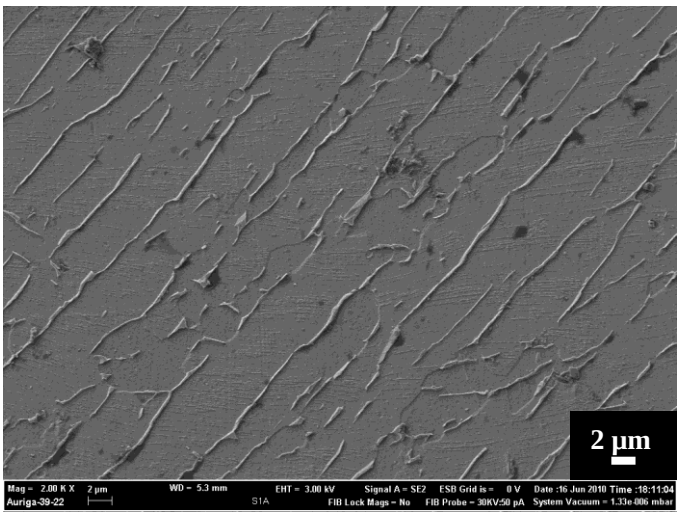


Figure 4.5: FESEM image of Ti6Al4V after embedment process for S1

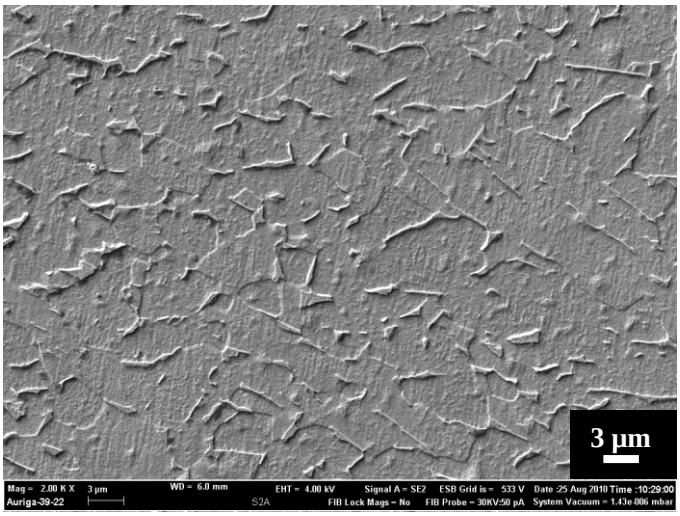


Figure 4.6: FESEM image of Ti6Al4V after embedment process for S2

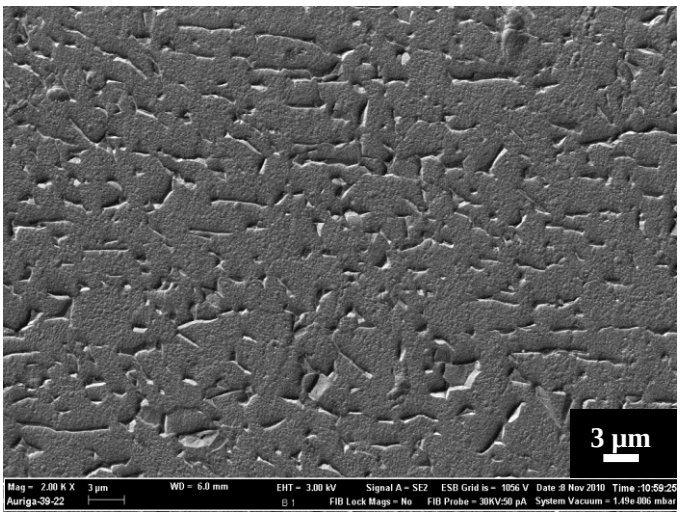


Figure 4.7: FESEM image of Ti6Al4V after embedment process for S3

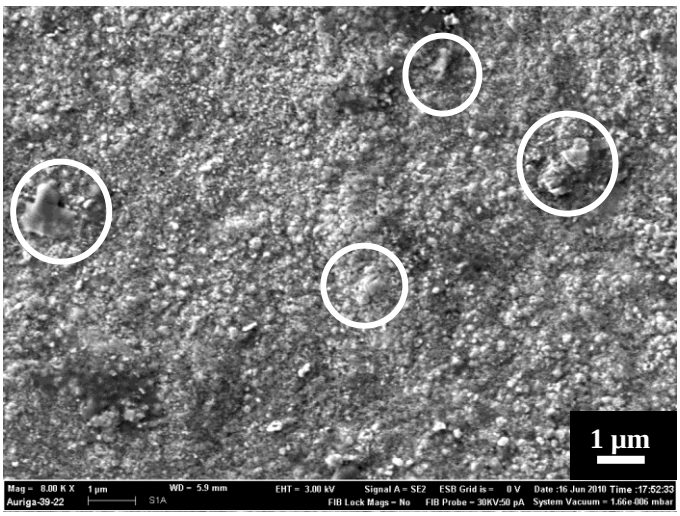


Figure 4.8: Surface morphology of HA embedded surface for S1

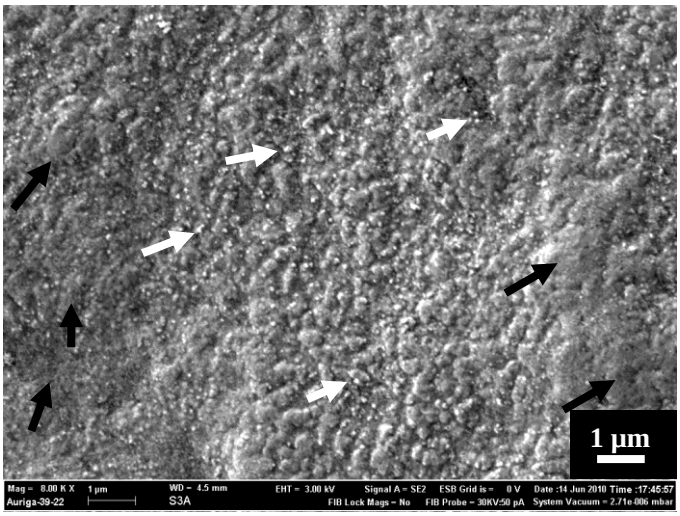


Figure 4.9: Surface morphology of HA embedded surface for superplastic S3

The cross-sectional view for S1 and superplastic S3 samples are presented in Figure 4.10 and 4.11, respectively with the embedded layer thickness represented in nanometres. The HA embedded layers show an increase in layer thickness as the sample becomes superplastic. The layer increases from 189 nm in S1 to 249 nm in superplastic S3, which indicates that the superplastic deformation process certainly helps to thicken the HA layer thickness. Two main elements which contribute to the formation of a thicker HA layer are higher applied stress (refer Figure 4.3) and finer grain substrate. High applied stress is needed to give good compaction to the HA powders, whereas a

fine grain substrate accelerates the diffusion of Ti onto the HA layer, which gives good adherence effects in the HA powders. This is similar to the effect when HA is mixed with Ti powder, which produces a stronger and tougher composite. The diffusion of elements is discussed further in subsequent paragraphs.

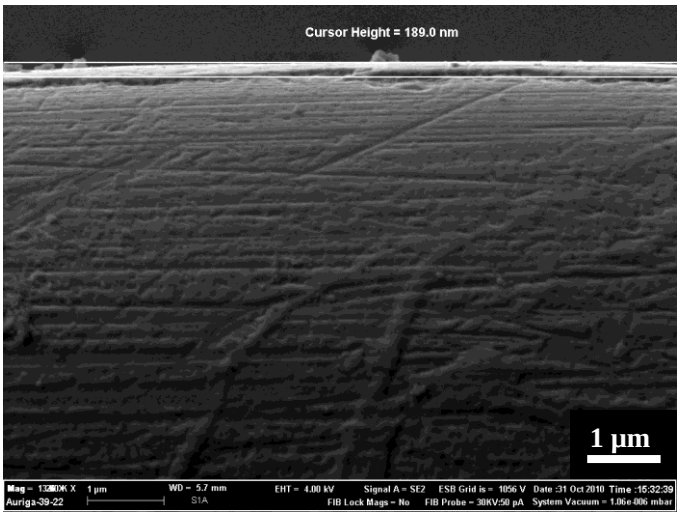


Figure 4.10: Cross-sectional FESEM image of HA embedded layer for S1

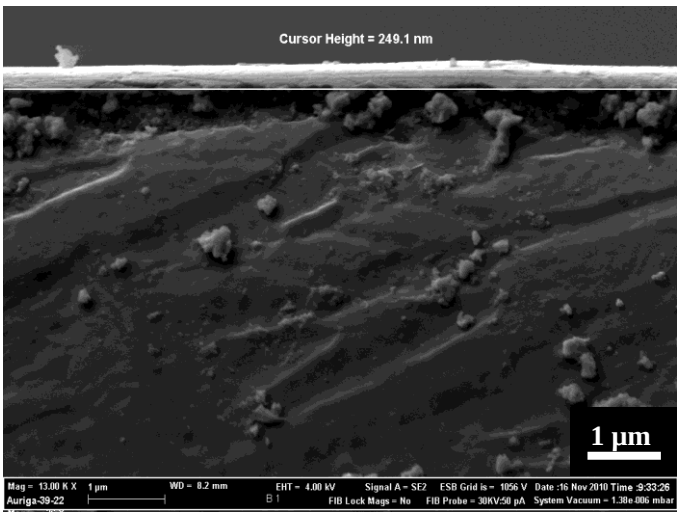


4.11: Cross-sectional FESEM images of HA embedded layer for superplastic S3

The hardness of the embedded surface and substrate for S1 and superplastic S3 samples is shown in Figure 4.12. The hardness of the embedded surface for superplastic S3 is relatively high compared with S1, indicating that the HA layer is denser.

Additionally, the hardness of the superplastic S3 substrate is high due to the fine grains obtained, which signifies that the substrate is ductile and tougher. As discussed earlier, the higher pressure applied during superplastic embedment and the higher diffusion rate of Ti in the superplastic sample contribute to the denser embedded layer.

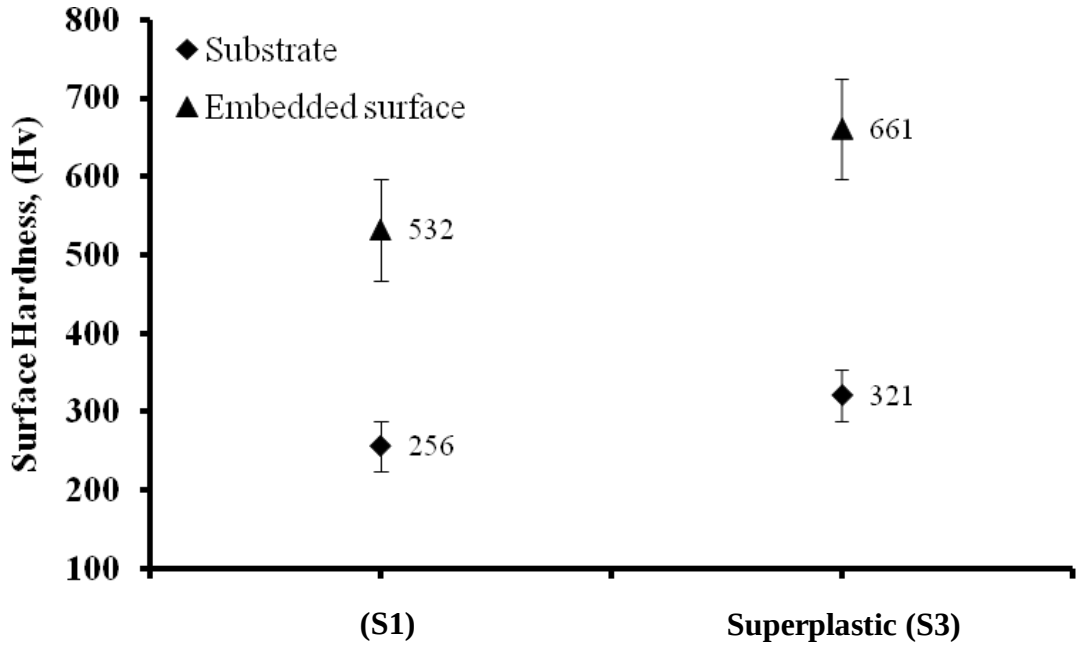


Figure 4.12: Hardness of substrates and embedded surfaces at different conditions

The X-ray diffraction (XRD) patterns are shown in Figure 4.13. It can be clearly seen that the XRD pattern for the heated HA powders under S1 and superplastic S3 conditions are similar to the XRD patterns for pure HA (Figure 4.13 (d), (e) and (a)). HA did not compose and maintained its original structure, after when heated under the specified conditions.

For the HA layer in S1 (Figure 4.13 (b)), HA peaks are not observed and relatively weak XRD lines corresponding to $TiO_2$ (rutile) are identified. The $TiO_2$ phase is influenced by the presence of Ti on the embedded layer and is also probably due to

the long exposure time during the embedment process. This suggests that HA was decomposed during the process. The XRD pattern for superplastic S3 however, shows relatively weak HA lines. This suggests that HA was not totally decomposed and was retained during the process. The weak HA lines may also be due to the nanometre thickness of the HA layer, since good XRD peaks of HA are unattainable for thin coatings (Pleshko et al., 1991; Xiong et al., 2010).

It is very common for HA to decompose into other by-products when mixed with Ti (Chu et al., 2006; Nath et al., 2009). The decomposition depends on several factors such as temperature and exposure time. In this study, the process duration for S1 and superplastic S3 samples is 150 min and 90 min, respectively. It is suggested that the decomposition of HA in S1 sample is due to the longer exposure time when the HA powders are mixed with the Ti substrate. HA is retained in superplastic S3 as the process duration is relatively much shorter. This confirms that relatively short exposure time for HA powders mixed with Ti will retain the crystallinity and phase purity of HA.

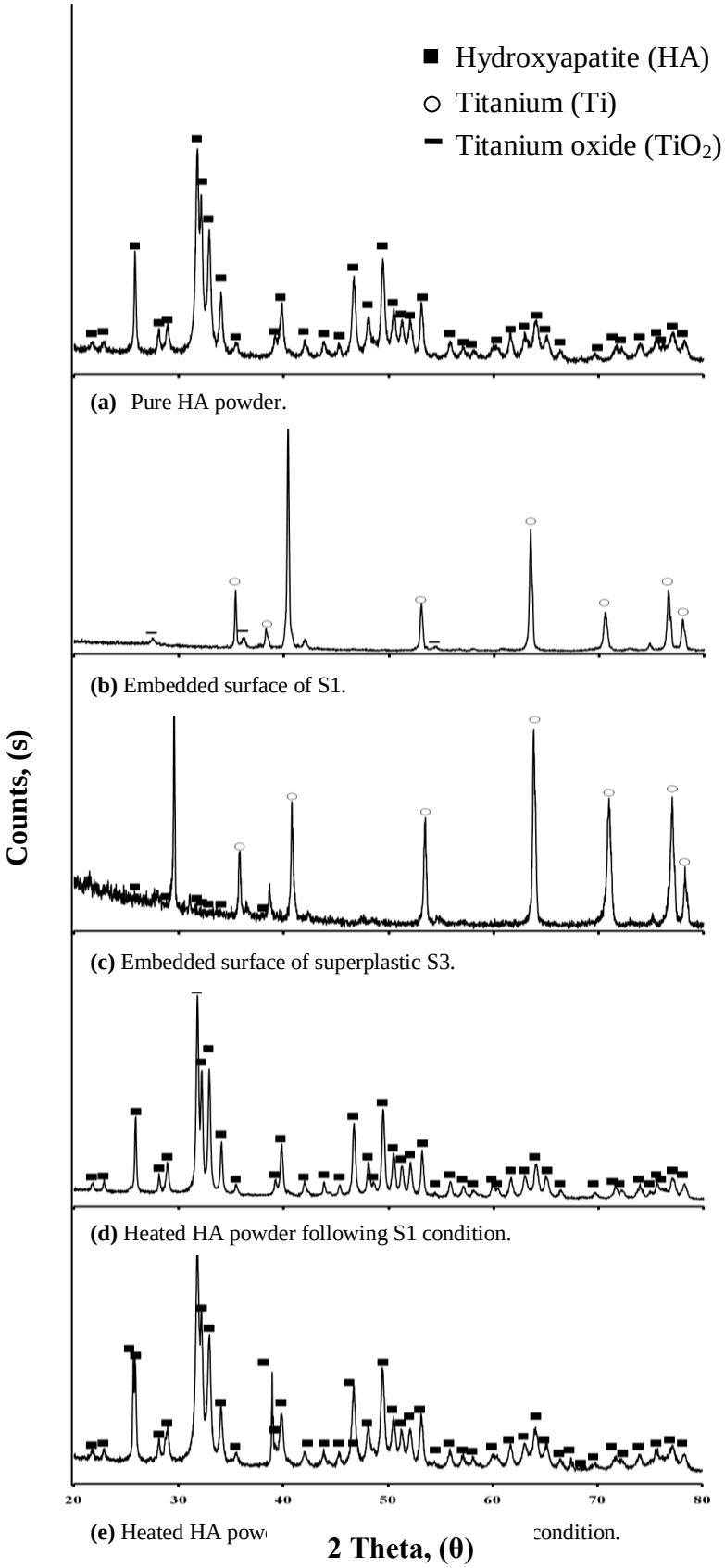


**(a)** Pure HA powder.

**(b)** Embedded surface of S1.

**(c)** Embedded surface of superplastic S3.

**(d)** Heated HA powder following S1 condition.

**(e)** Heated HA pow condition.

Figure 4.13: XRD patterns of HA powder and embedded surface at different conditions

Since strong Ti lines were identified significantly in the XRD patterns of Figure 4.13 b and c, the diffusion of the main substrate element, Ti into the embedded HA layer was analysed using Energy-Dispersive X-ray (EDX) spectroscopy. Figure 4.14 shows the intensities of Ti in S1 and superplastic S3 samples. The amount of Ti is determined to be 51 wt% and 53 wt% for S1 and superplastic S3, respectively. The percentage amount of Ti in superplastic S3 is higher although the process duration is shorter.

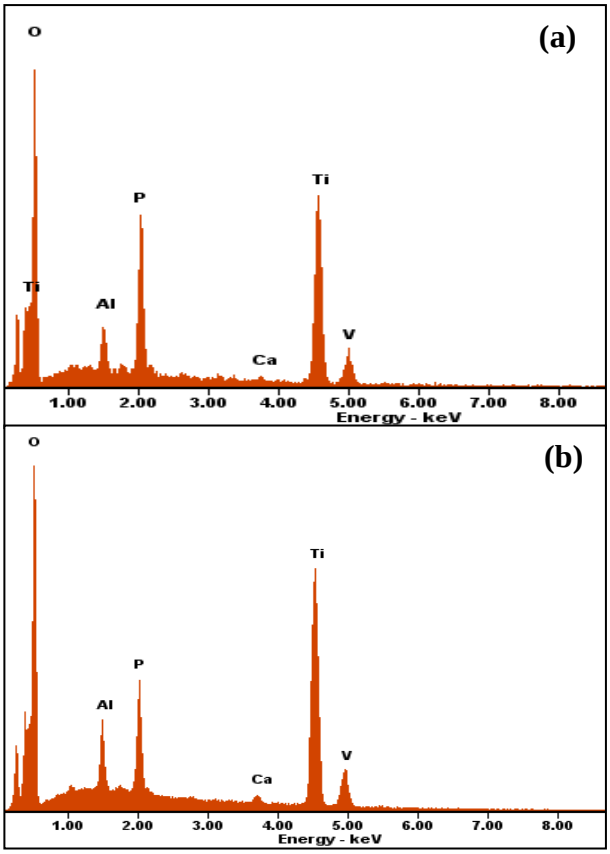


Figure 4.14: EDX spectrum of: (a) S1 and (b) superplastic S3 after embedment

Figure 4.15 illustrates the line scanning profile of Ti element across the substrate/embedded layer interface after the embedment process for superplastic S3. The figure shows that the amount of Ti decreases gradually from the titanium substrate

to the HA layer. This supports the fact that interdiffusion of Ti occurs from the substrate to the layer.

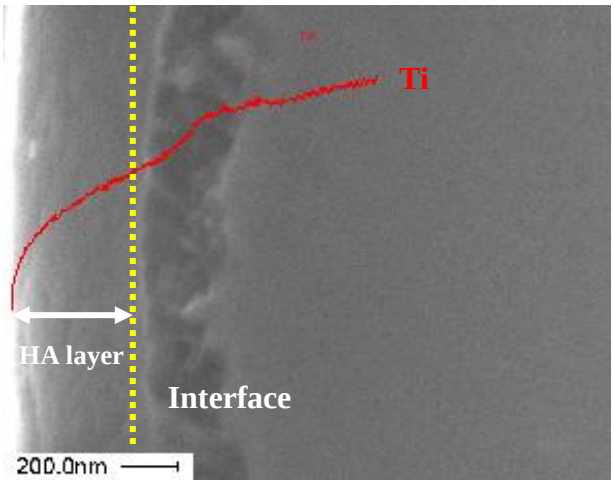


Figure 4.15: EDX line analysis of Ti element on the cross-section of HA layer for superplastic S3

## 4.3 Wear test in simulated body fluid (SBF)

Simulated body fluid (SBF) has been widely used for the investigation of in vitro bioactivity because the inorganic ion concentrations in SBF are close to those in blood plasma. Wear tests were performed in SBF in order to evaluate the adherent strength of the HA layer and strength between the HA layer and the substrate (interfacial strength) for biomedical applications. The bonding strength between the layer and the substrate should be sufficiently high to withstand the interfacial stresses encountered in *in vivo* environment. This is because the embedded layer (HA or HA/Ti layer) should provide a bioactive surface on a metal implant for bone in growth.

### 4.3.1 Wear behaviour of S1

Figure 4.16 ((a) – (d)) presents the surface morphologies for S1 sample before and after wear tests at different pressures, and the cross-sectional views are shown in Figure 4.17 ((a) – (d)). At a low pressure (0.05 MPa), the morphology of the worn surface (Figure 4.16 (b)) indicates that the rough unmelted HA particles in S1 are gouged out with the thickness of the embedded layer slightly removed, as shown in Figure 4.17 (b). However, the surface is still relatively rough, indicating that the unmelted particles are not completely worn out. When the pressure was increased to 0.2 MPa, a smoother surface is attained, without signs of unmelted particles (Figure 4.16 (c)). However, under this pressure condition, the embedded layer is removed significantly from the substrate (Figure 4.17 (c)). As the pressure further increased (0.4 MPa), spalling of the HA layers can be observed (Figure 4.16 (d)), and from the cross-sectional view, the layer is no longer visible (Figure 4.17 (d)).

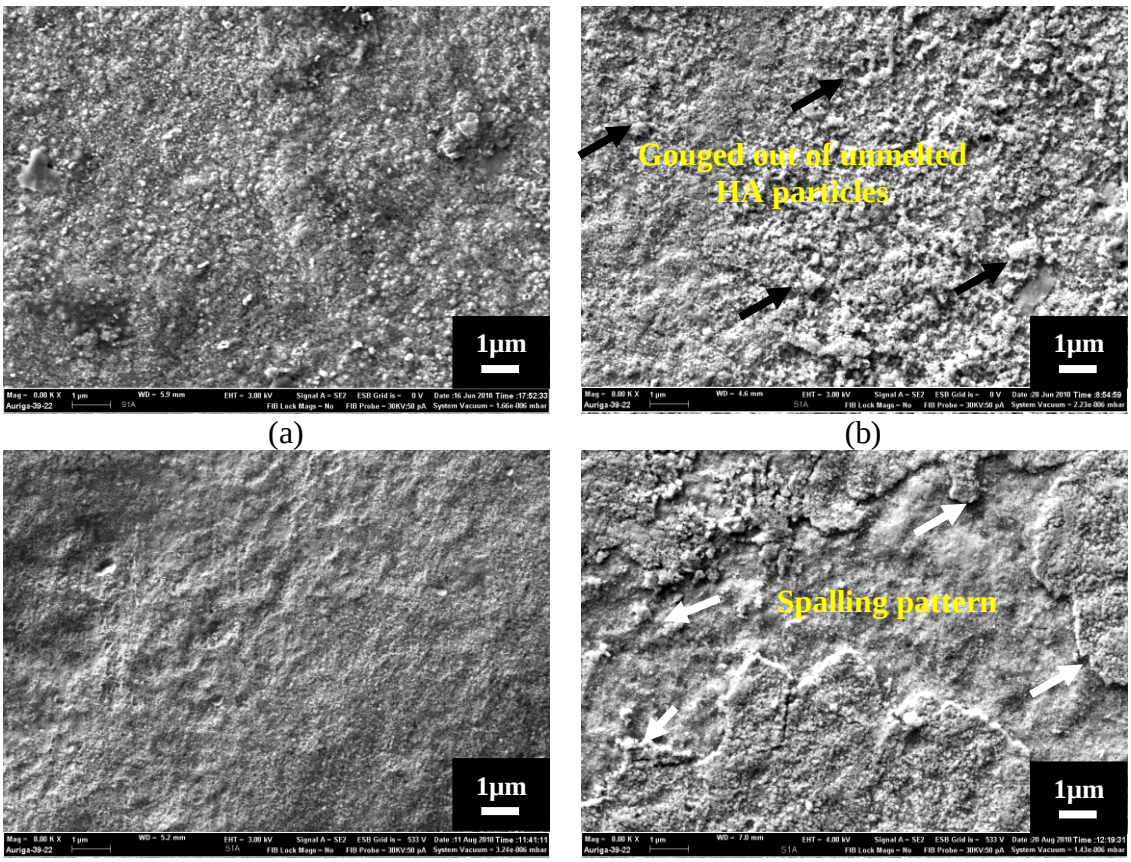


(a) (b)

(c) (d)

Figure 4.16: Surface morphology of embedded HA layer for S1: (a) before wear, (b) 0.05 MPa for 30 min (~2177 m), (c) 0.2 MPa for 30 min (~8709 m) and (d) 0.4 MPa for 30 min (~17417 m)

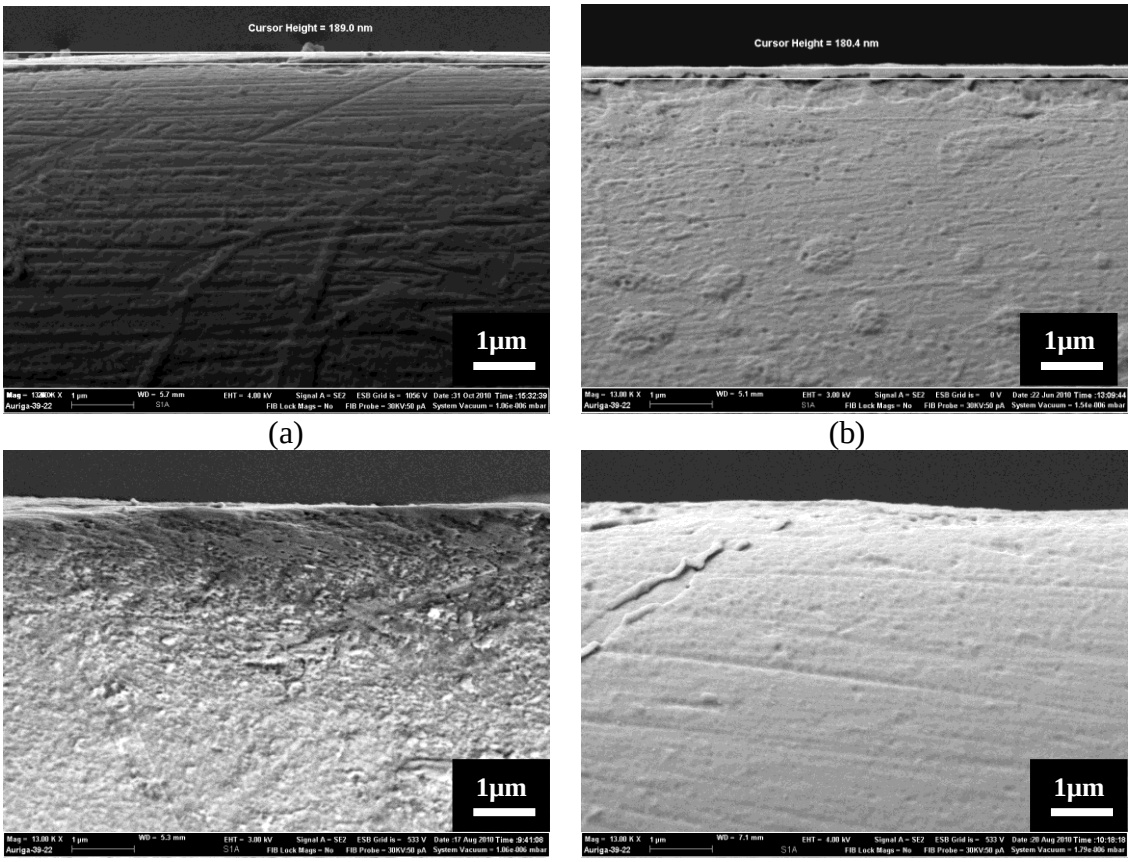


(a) (b)

(c) (d)

Figure 4.17: Cross-sectional view of embedded HA layer for S1: (a) before wear, (b) 0.05 MPa for 30 min (~2177 m), (c) 0.2 MPa for 30 min (~8709 m) and (d) 0.4 MPa for 30 min (~17417 m)

### 4.3.2 Wear behaviour of superplastic S3

Figures 4.18 and 4.19 show the surface morphologies and cross-sectional views of the superplastic S3 sample after wear tests under similar conditions. At the lowest pressure (0.05 MPa), the surface becomes smoother and a slight removal of layer is observed (Figure (4.18 and 4.19) (b)). This phenomenon is quite similar to the one occurred during the wear tests of S1, whereby the unmelted HA particles are worn out from the surface. Although a reduction in HA layer thickness is observed upon further increase in pressure (0.2 and 0.4 MPa), the surface morphology is relatively maintained (Figure 4.18 (c) and (d)). At the highest pressure (0.4 MPa), wear tracks can be identified on the surface, but, the HA layer remains intact with nearly no signs of HA

layer thickness reduction (Figure (4.18 and 4.19) (d)). However, a different behaviour is observed for S1, whereby a total removal of the HA layer occurs.

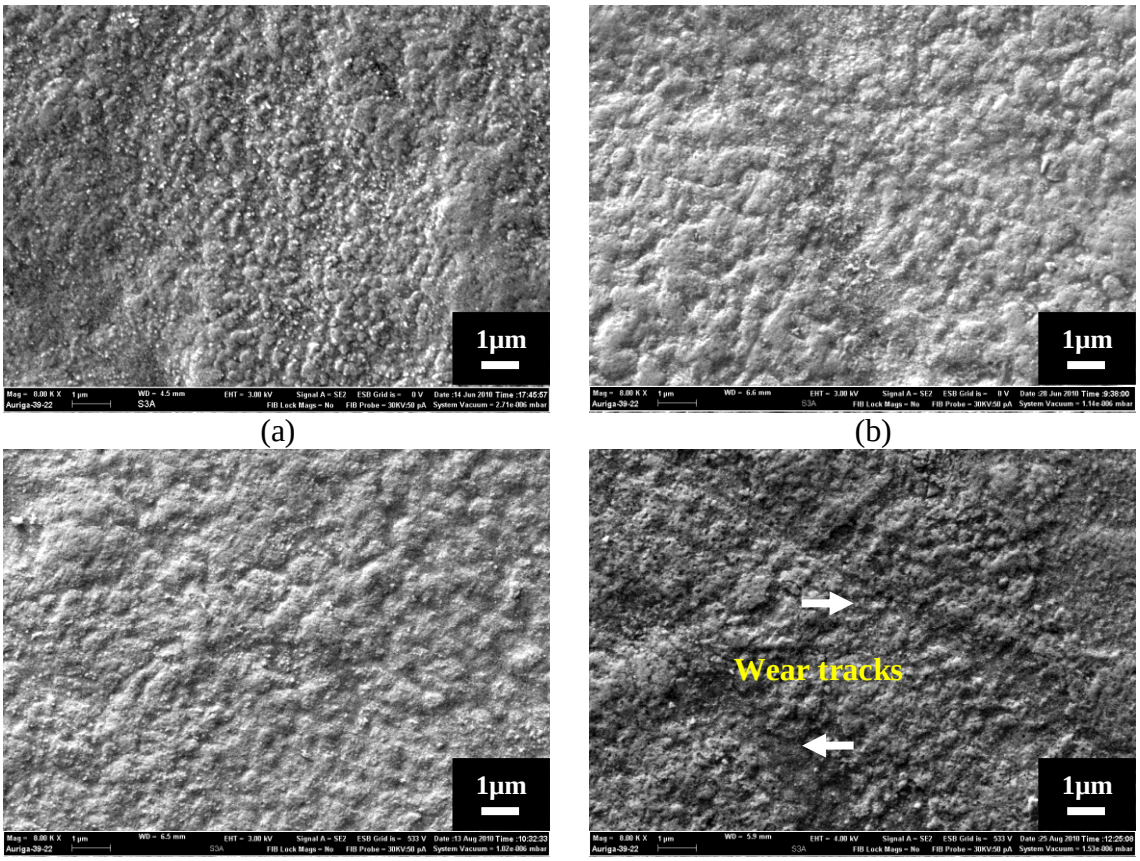


(a) (b)

(c) (d)

Figure 4.18: Surface morphology of embedded HA layer of superplastic S3; (a) before wear, (b) 0.05 MPa for 30 min (~2177 m), (c) 0.2 MPa for 30 min (~8709 m) and (d) 0.4 MPa for 30 min (~17417 m)

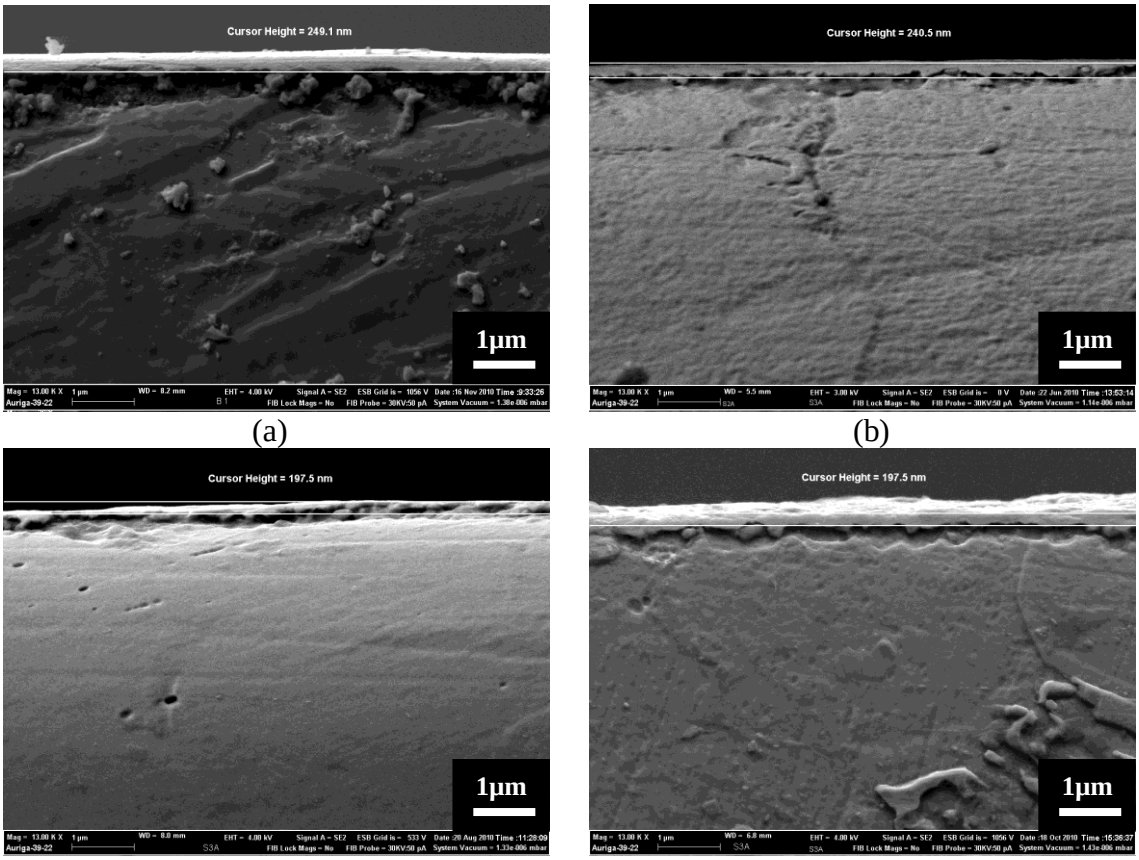


Figure 4.19: Cross-sectional view of embedded HA layer of superplastic S3; (a) before wear, (b) 0.05 MPa for 30 min (~2177 m), (c) 0.2 MPa for 30 min (~8709 m) and (d) 0.4 MPa for 30 min (~17417 m)

From the above results, one can say that the wear properties of the HA layer in superplastic S3 sample is superior compared with the non-superplastic S1 sample. The results reveal that, the adherent strength of HA layer and the interfacial strength improve significantly by the superplastic embedment process employed in this study. The diffusion of Ti from the fine grain substrate and the high applied stress during compression lead to the formation of dense HA/Ti composite, which improves the HA adherent strength. As for the interfacial strength, the continuous pressing during embedment process is expected to superplastically deform the surface asperities of the substrate, which consequently produces strong bonds between the HA layer and substrate.

The process is similar to the solid-state diffusion bonding concept. It is understood that during the early stage of solid-state diffusion bonding process, the asperities on each of the faying surfaces deform plastically as the pressure is applied. In the following stage, creep and diffusion of atoms mainly occur. In this study, the surface asperities of the Ti-6Al-4V substrate can be easily plastically deformed by continuous pressing, which expedites the embedment between HA powder and substrate. The grain refinement of alloy during the superplastic embedment process accelerates the following diffusion stage. The combination of these two elements; (i) superplastic deformation of substrate surface asperities and (ii) fine grain, is considered to be the primary reason for the strong layer produced.

It is crucial to have strong adherent strength for the HA layer due to the fact that removal of debris particles can raise safety concerns (Bauer et al., 1994; Bloebaum et al., 1994). At the same time, the interfacial strength is also important. The interfacial strength can be considered as the roots of a tree. Without strong roots, even a good tree can collapse. In this case, both of the issues; (i) adherent strength of the HA layer and (ii) interfacial strength are being addressed satisfactorily through the superplastic embedment process. Furthermore, the crystal structure of HA is maintained through a shorter process duration.

## 4.4 High Temperature Deformation of Superplastic S3 Under Different Conditions

The combinations of titanium and bioactive ceramics render titanium coated with hydroxyapatite (HA) valuable for medical applications (Balazic et al., 2007; Nonami et al., 1998; Onoko et al., 2008). In orthopaedic technology development, HA coatings are applied after the devices are formed into various shapes. It is known that deformation process does not occur after coatings are applied. However, in this manner, uniform coating is difficult to attain, especially when complex-shaped devices are involved. Additionally, dissolution process easily occurrs, which may lead to the disintegration of coatings, which hinders the fixation of implant to the host tissue (Ishikawa et al., 1997; Zhang et al., 2006). Hence, the feasibility of forming Ti alloys embedded with HA nanolayers (superplastic S3 sample) at high temperature compression process was investigated, as an approach to achieve reliable implant-to-bone fixation.

### 4.4.1 Compression of Superplastic S3

Figure 4.20 shows the stress-strain curves of the compressed superplastic S3 samples at different degrees of deformation. It is clearly seen that the curves exhibit a similar pattern, whereby the applied stress increases steadily with increasing degree of deformation. The maximum stress for 10, 20 and 30% deformation is found to be 50, 89 and 112 MPa, respectively. The compression time for the three conditions is 1, 2 and 3 min, respectively.

The microstructures of the sample compressed at different degree of deformation are presented in Figures 4.21 – 4.23. It is clearly seen that the two-phase microstructure

consisting of α and β phase is retained even after high temperature deformation. The average grain size of the sample after 10, 20 and 30 % deformation is 2.7 ± 0.5, 3.0 ± 0.5 and 3.4 ± 0.5 µm, respectively. Although the grain size increases with deformation, it is still considered as superplastic condition since the average grain size does not exceed 10 µm, which is known as one of the basic requirements for superplasticity (Giuliano, 2008). Table 4.3 summarizes the properties of superplastic S3 sample after the compression process.

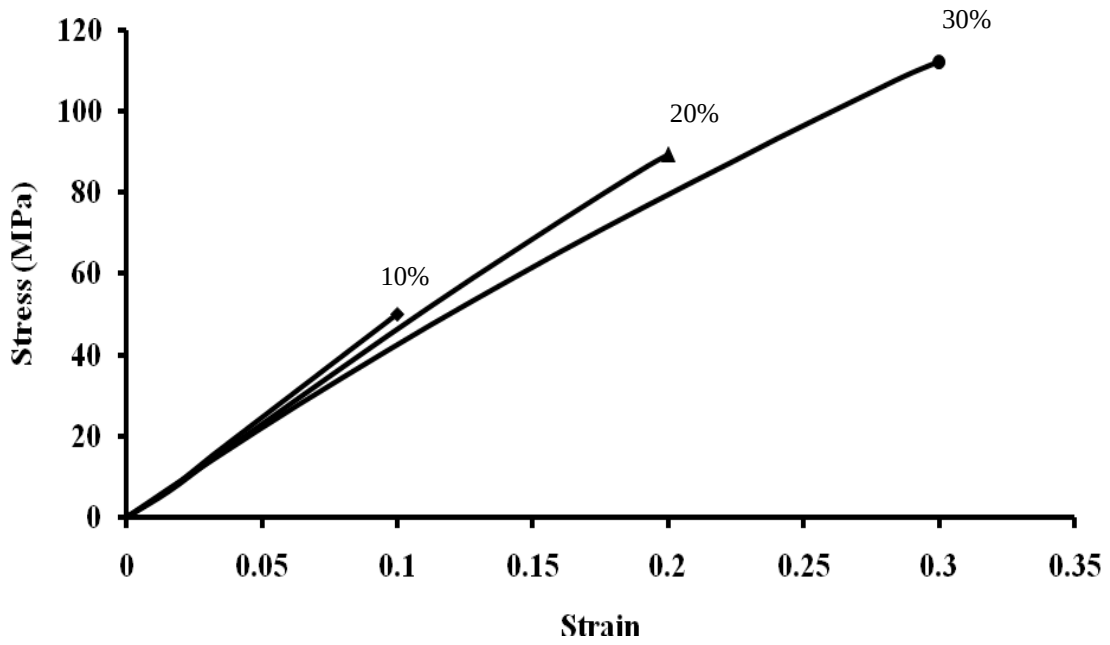


Figure 4.20: Typical stress-strain curves of the compression process for samples under different conditions at a strain rate of $1.6 \times 10^{-3}$ $s^{-1}$ and temperature of 1200K

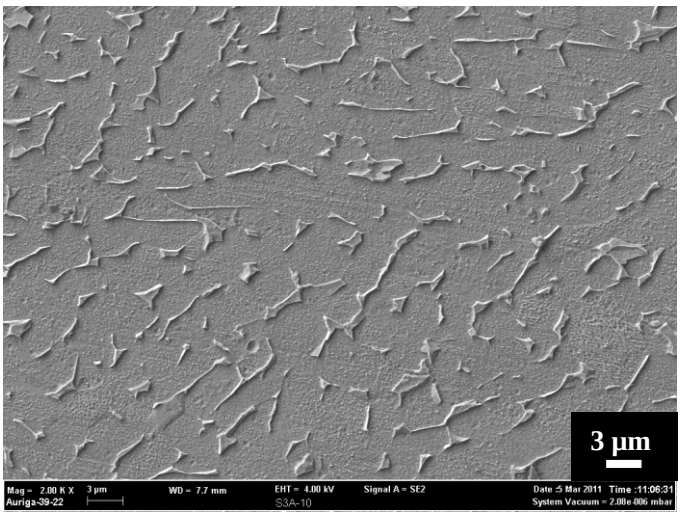


Figure 4.21: FESEM image of superplastic S3 after 10% compression

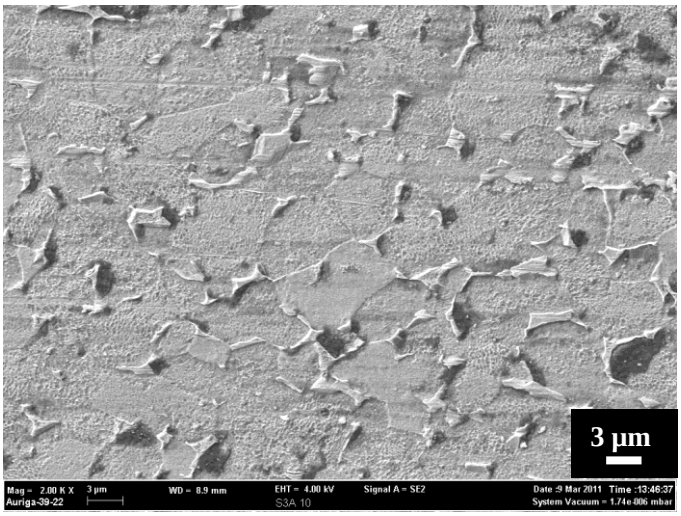


Figure 4.22: FESEM image of superplastic S3 after 20% compression

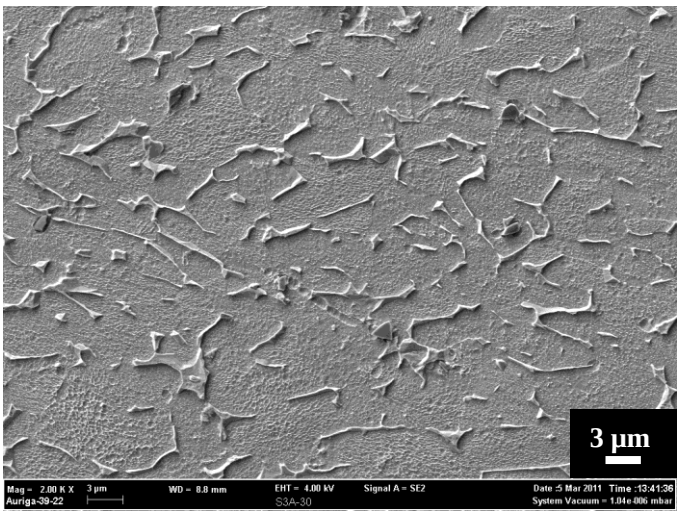


Figure 4.23: FESEM image of superplastic S3 after 30% compression

Table 4.3: Properties of superplastic S3 after compression process under various deformation degree at a strain rate of $1.6 \times 10^{-3}$ $s^{-1}$

| **Deformation degree (%)** | **10** | **20** | **30** |
|---|---|---|---|
| **Maximum load, MPa** | 50 | 90 | 113 |
| **Time, min** | 1 | 2 | 3 |
| **Grain size, µm** | 2.7±0.5 | 3.0±0.5 | 3.4±0.5 |

### 4.4.2 Deformation Behaviour and Characterizations

Figures 4.24 and 4.25 exhibit the cross-sections and surface morphologies of the samples before and after deformation, respectively. The HA layer thickness is approximately 249 nm before deformation (Figure 4.24a). The surface is relatively smooth, with well-melted HA covering most of the area (Figure 4.25a (i)). Higher magnification figure shows the presence of fine unmelted HA particles in some areas (Figure 4.25a (ii)). The HA layer thickness reduces to approximately 241 nm after a deformation of 10% (Figure 4.24b). The initially smooth surface appears slightly rougher, whereby gouged out HA particles are observed, as indicated by the circles in Figure 4.25b (ii). The HA layer thickness reduces further to 223 nm at a deformation degree of 20% (Figure 4.24c). Micro cracks can be observed in certain areas on the surface (Figure 4.25c (i and ii)). The HA layer thickness reduces to 207 nm when the deformation is increased to 30% (Figure 4.24d). Delaminations and total removals of HA layer from the substrate's surface are noticeable in certain areas (Figure 4.25d (i and ii)).

From these results, it is seen that when the deformation degree is increased, the HA layer is exposed to higher compression stress, which eventually leads to crackings, delaminations and total removals of the HA layer. However, based on the observations in Figures 4.24 and 4.25, the HA layer remains intact even after a deformation of 30%. Additionally, it is found out that the cracks and delaminations are revealed only when the embedded HA surface was examined under high magnifications of ×4000 and ×8000, which indicates that the magnitudes of failure may be very small. Under low magnification (×100) (Figure 4.26 (a - c)), it can be observed that the surface morphologies for the three samples are nearly identical.

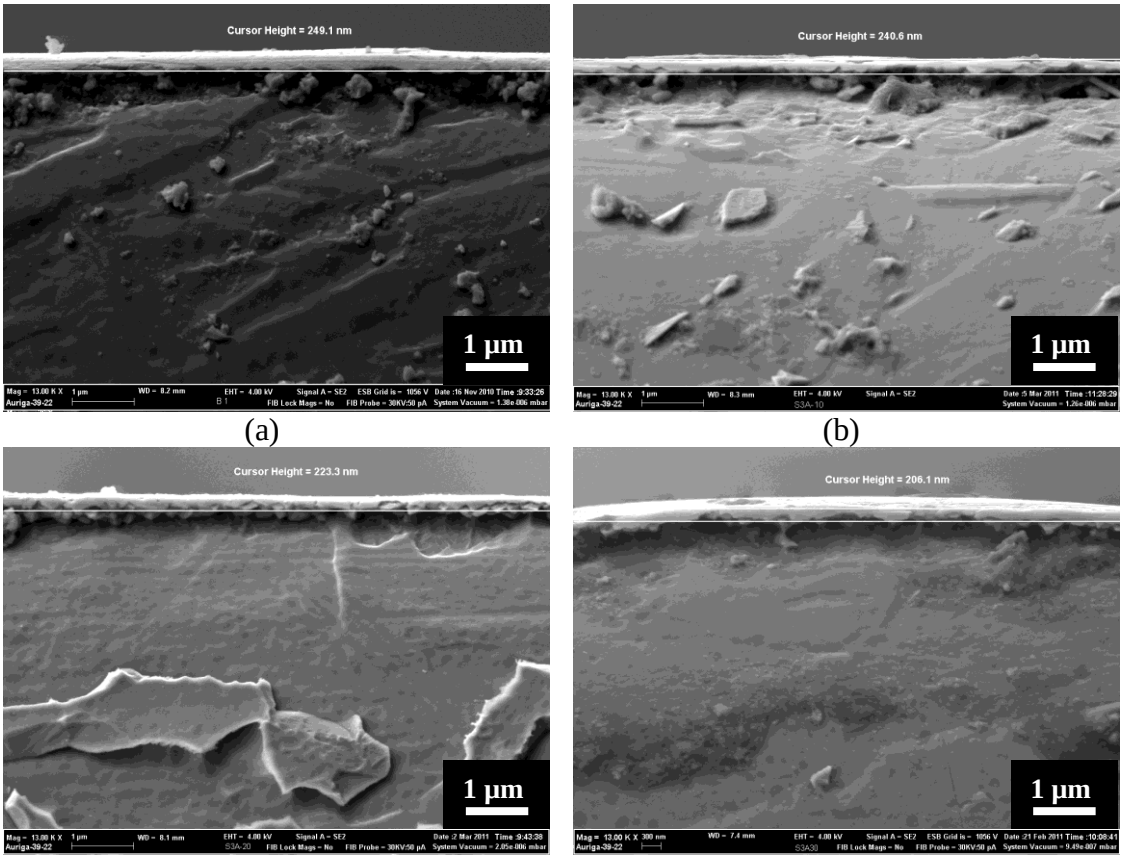


Figure 4.24: FESEM images of HA embedded layer for superplastic S3 (a) before deformation, (b) after 10% deformation, (c) after 20% deformation and (d) after 30% deformation

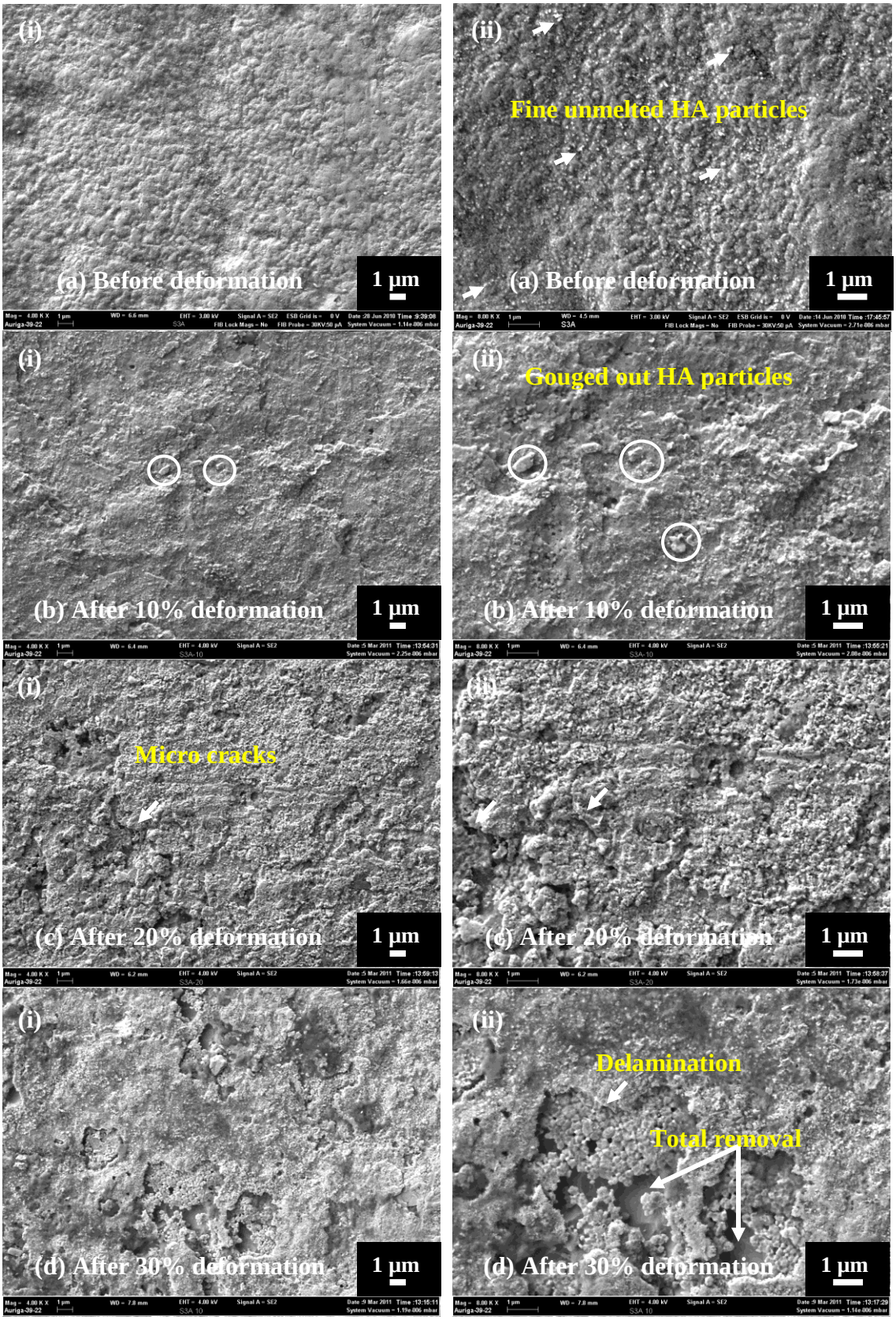


Figure 4.25: Surface morphology of superplastic S3 before and after deformation. (i) Magnification at ×4000 and (ii) Magnification at ×8000

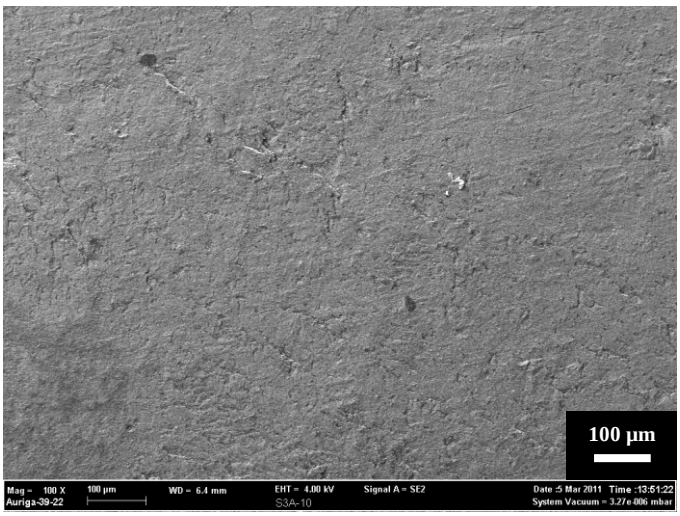


(a) After 10% deformation

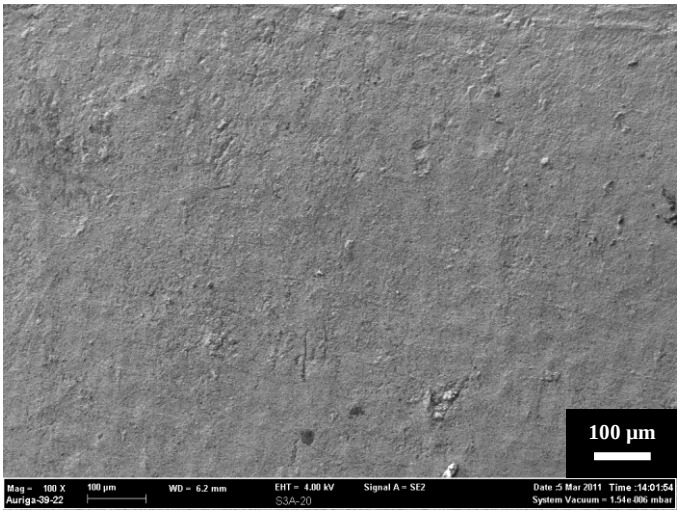


(b) After 20% deformation

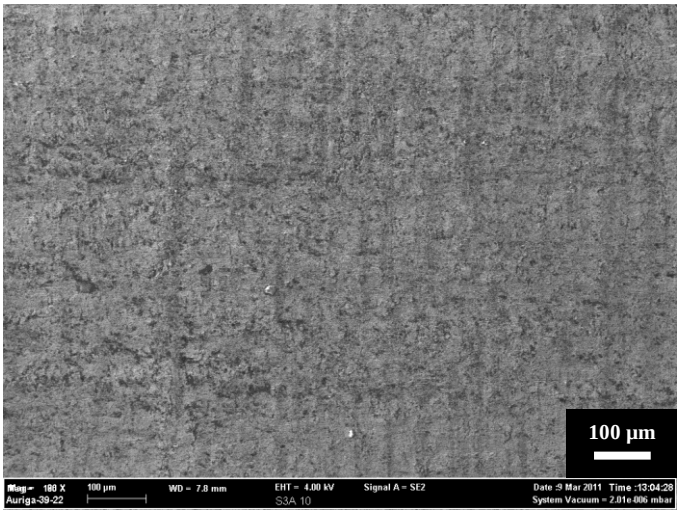


(c) After 30% deformation

Figure 4.26: Surface morphology of deformed superplastic S3 at low magnification of ×100

The hardness of the embedded surface and titanium substrate after the deformation is shown in Figure 4.27. The surface hardness of the deformed samples decreases with increasing degree of deformation. However, the surface hardness of deformed samples is relatively high compared with the substrate's hardness, which further shows the intactness of the HA embedded layer. In addition increasing the degree of deformation decreases the hardness of the substrates due to grain growth (refer to Figure 4.21 – 4.23).

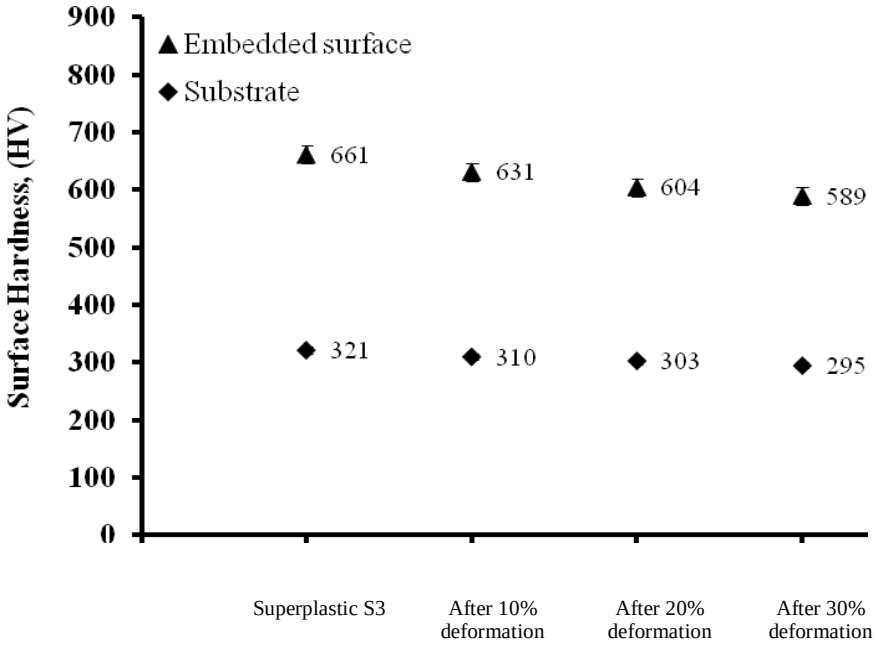


Figure 4.27: Hardness of embedded surface and substrate of deformed superplastic S3 at different conditions

Figure 4.28 shows the XRD patterns of the embedded surface before and after deformation. The HA structure is retained after deformation. Further heating at 1200 K during the deformation process results in improved crystallinity, which is indicated by the strong HA line peaks, especially at around 40°. Kweh et al. stated that the crystallinity of HA increases when HA coatings are heat-treated (Kweh et al., 2002).

Thus, in this study, it is shown that to a certain degree, it is feasible to form Ti alloys superplastically embedded with HA nanolayers without deteriorating their properties. The concept used in this study will certainly expand the applications of superplasticity in this field.

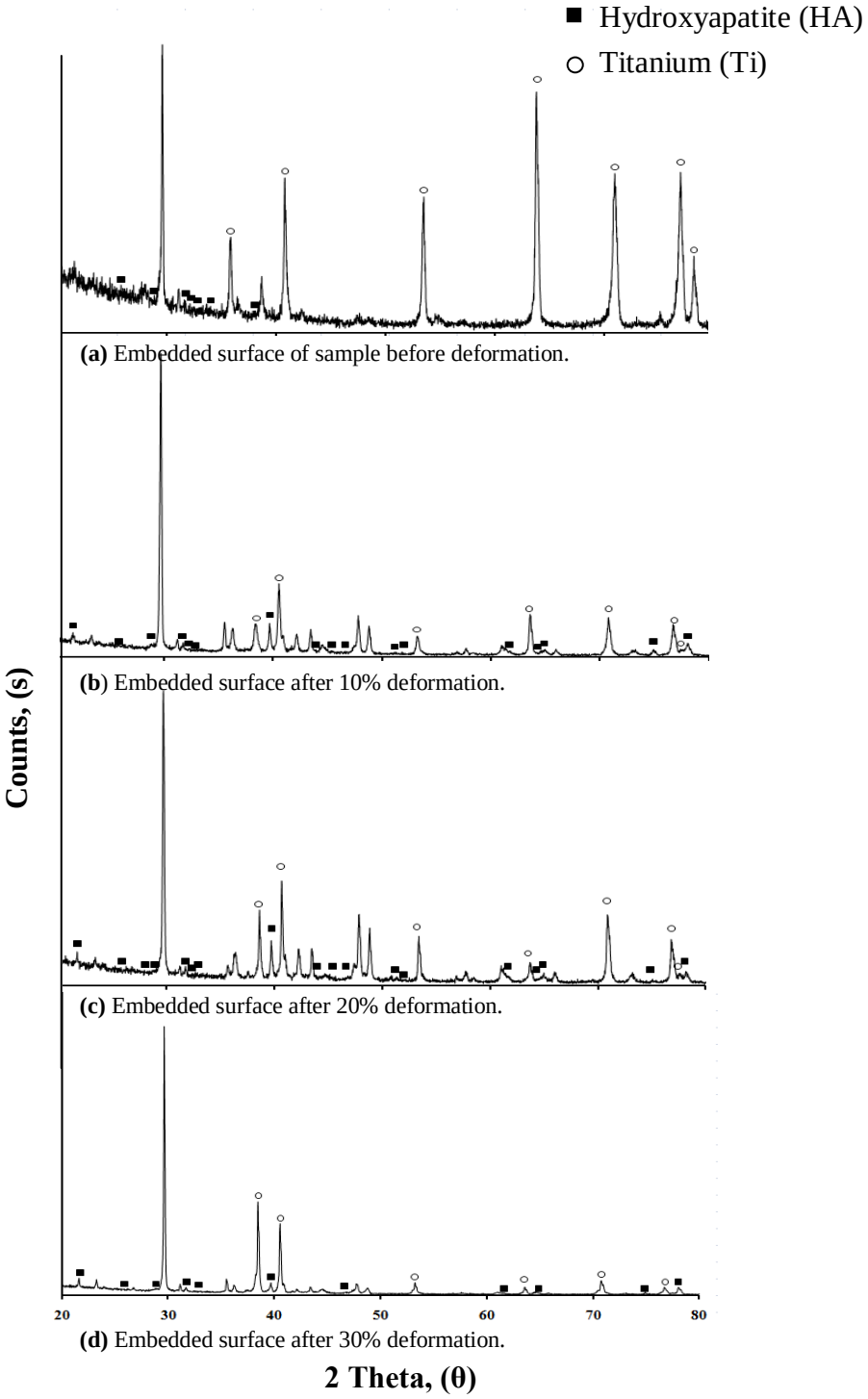


**(a)** Embedded surface of sample before deformation.

**(b)** Embedded surface after 10% deformation.

**(c)** Embedded surface after 20% deformation.

**(d)** Embedded surface after 30% deformation.

Figure 4.28: XRD pattern of embedded surface at different condition

# CHAPTER 5

# CONCLUSIONS AND RECOMMENDATIONS

## 5.1 Conclusions

The following conclusions can be drawn from this study:

(1) Nanometre – thickness HA layers are obtained successfully through the embedment process, regardless of the conditions.

(2) The optimum condition for superplastic embedment is achieved at a strain rate of $1 \times 10^{-4}$ $s^{-1}$ (superplastic S3 sample), which is equivalent to process duration of 90 min.

(3) The surface hardness of the superplastic sample (661±0.5 HV) is higher than the non-superplastic sample (532±0.5 HV) due to the formation of denser and thicker HA layer.

(4) XRD results show that HA is retained after the embedment process for superplastic sample as the process duration is relatively much shorter.

(5) EDX and line scan analyses show that a significant amount of Ti diffuses onto the HA layer for superplastic sample, leading to formation of dense HA/Ti composite layer.

(6) Wear tests under SBF condition reveal that the adherent strength of HA and interfacial strength between the HA layer and substrate is enhanced significantly in superplastic sample as compared with the non-superplastic sample.

(7) The overall results of high temperature deformation behaviour for superplastic S3 sample show that the HA layer is strongly intact to the substrate's surface even after the deformation process.

(8) XRD investigations of the deformed sample illustrate that the HA structure is retained effectively, even after deformation at high temperature.

## 5.2 Recommendations

The recommendations for future research are listed as follows:

(1) Since Ti6Al4V is highly reactive to nature, future experiments should be carried out under vacuum conditions during the embedment process.

(2) More evaluations can be carried out on the strength of the embedded layer after high temperature deformation using different testing methods such as scratch and fatigue tests.

(3) Investigations of the apatite growth for the embedded HA nanolayer can also be carried out in *in-vitro*.

# REFERENCES


Adibah Haneem Mohamad Dom, Iswadi Jauhari, Yazdanparast, S., & Hidayah Mohd Khalid. (2010). Embedment of HA/Ti composite on superplastic titanium alloy (Ti-6Al-4V). *Materials Science and Engineering: A, 527*(21-22), 5831-5836.

Balazic, M., Kopac, J., & Ahmed, W. (2007). Review: titanium and titanium alloy applications in medicine. *International Journal of Nano and Biomaterials, 1*(1), 3-34.

Bauer, T. W., Taylor, S. K., Jiang, M., & Medendorp, S. V. (1994). An indirect comparison of third-body wear in retrieved hydroxyapatite-coated, porous, and cemented femoral components. *Clinical Orthopaedics and Related Research, 298*, 11-8.

Bigi, A., Boanini, E., Bracci, B., Facchini, A., Panzavolta, S., Segatti, F., & Sturba, L. (2005). Nanocrystalline hydroxyapatite coatings on titanium: a new fast biomimetic method. *Biomaterials, 26*(19), 4085-4089.

Bloebaum, R. D., Beeks, D., Dorr L. D., Savory, C. G., Du Pont, J. A., & Hofmann, A. A. (1994). Complications with hydroxyapatite particulate separation in total hip arthroplasty. *Clinical Orthopaedics and Related Research, 298*, 19-26.

Bothe, R. T., Beaton, L. E., & Davenport, H. A. (1940). Reaction of bone to multiple metallic implants. *Surgery, Gynecology and Obstetrics, 71*, 598-602.

Boyer, R. R. (1996). An overview on the use of titanium in the aerospace industry. *Materials Science and Engineering: A, 213*(1-2), 103-114.

Brados, B. I. (2006). Titanium and Titanium Alloys in Medical Applications. In *The encyclopedia of materials science and engineering* (Vol. 7, pp. 5099-5103). Japan: Encyclopedia of Materials Science and Engineering.

Broadwell, R. G. (2006). Titanium and Titanium Alloys: Selection. In *The encyclopedia of materials science and engineering* (Vol. 7, pp. 5104-5106). Japan: Encyclopedia of Materials Science and Engineering.

Brown, B. (2000). A Theory for Stretchiness. In *Elastic Instability of Grain Boundaries and the Physical Origin of Superplasticity*. Retrieved October 03, 2008, from http://focus.aps.org/story/v6/st10

Chandra, N. (2002). Constituve behaviour of superplastic materials. *International Journal of Non-Linear Mechanics, 37*(3), 461-484.

Chen, J., Tong, W., Cao, Y., Feng, J., & Zhang, X. (1997). Effect of atmosphere on phase transfoemation in plasma-sprayed hydroxyapatite coatings during heat treatment. Journal *of Biomedical Materials Research, 34*(1), 15-20.

Choubey, A., Basu, B., & Balasubramaniam, R. (2004). Tribological behaviour of Ti-based alloys in simuated body fluid solution at fretting contacts. *Materials Science and Engineering: A*, *379*(1-2), 234-239.

Chu, C., Xue, X., Zhu, J., & Yin, Z. (2006). Fabrication and characterization of titanium-matrix composite with 20 vol% hydroxyapatite for use as heavy load-bearing hard tissue replacement. Journal of Materials science: Materials in Medicine, 17(3), 245-251.

Cotell, C. M., Chrisey, D. B., Grabowski, K. S., Sprague, J. A., & Gossett, C. R. (1992). Pulse laser deposition of hydroxyapatite thin films on Ti-6Al-4V. *Journal of Applied Biomaterials*, *3*(2), 87-93.

De Jonge, L. T., Leeuwenburgh, S. C. G., Van Den Beucken, J. J. P., Te Riet, J., Daamen, W. F., Wolke, J. G. C., et al. (2010). The osteogenic effect of electrosprayed nanoscale collagen/calcium phosphate coatings on titanium. *Biomaterials*, *31*(9), 2461-2469.

Ding, R., Guo, Z. X., & Wilson, A. (2002). Microstructural evolution of a Ti-6Al-4V alloy during thermomechanical processing. *Materials Science and Engineering A*, *327*(2), 233-245.

Disegi, J.A. (2000). Titanium alloys for fracture fixation implants, injury. *International Journal of The Care of the Injured*, *31*, S-D14.

Dutrow, B. L., &Clark, C. M. (2011). X-ray Powder Diffraction (XRD). In *Geochemical Instrumentation and Analysis*. Retrieved April 13, 2011, from http://serc.carleton.edu/research_education/geochemsheets/techniques/XRD.html

Edington, J. W., Melton, K. N., & Cutler, C. P. (1976). Superplasticity. *Progress in Materials Science*, *21*(1-2), 61-170.

Efunda. (2002). Typical properties of Ti alloys. In General Information on Titanium Alloys. Retrieved July 20, 2007, from http://www.efunda.com/materials/alloys/titanium/properties.cfm

Froes, F. H., & Bomberger, H.B. (1985). The beta titanium alloys. *Journal of Metals*, *37*, 28-37.

Gallagher, L. (2004). Enhancement of cryogenically treated lacrosse shafts. (Independent Study - Dr. Jones, 2001). *Independent Student Paper*.

Ghosh, A. K., & Hamilton, C. H. (1979). Mechanical behaviour and hardening characteristics of a superplastic Ti-6Al-4V alloy. *Metallurgical Transactions A*, *10*(6), 699-706.

Giuliano, G. (2008). Constitutive equation for superplastic Ti-6Al-4V alloy. *Materials and Design, 29*(7), 1330-1333.

Gnanamoorthy, R., Mutoh, Y., & Mizuhara, Y. (1996). Fatigue crack growth behavior of quiaxed, duplex and lamellar microstructure γ-base titanium aluminides. *Intermetallics, 4*(7), 525-532.

Gordon England. (2008). Microhardness Test. In Surface Engineering Forum. Retrieved February 02, 2008, from http://www.gordonengland.co.uk/hardness/microhardness.htm

Hench, L. L. (1998). Bioceramics. *Journal of the American Ceramic Society, 81*(7), 1705-1728.

Henkel, D. P., & Pense, A. W. (2001). *Structures and Properties of Engineering Materials – Materials Science & Engineering*. Location: McGraw-Hill Publishing Co.

Ishikawa, K., Miyamoto, Y., Nagayama, M., & Asaoka, K. (1997). Blast coating method: new method of coating titanium surface with hydroxyapatite at room temperature. *Journal of Biomedical Materials Research, 38*(2), 129-134.

Joshi, A. (2002). *Introduction to superplastic forming process*. Indian Institute of Technology, Bombay.

Karasevskaya, O. P., Ivasishin, O., M., Semiatin, S. L., & Matviychuk, Y. V. (2003). Deformation behavior of beta-titanium alloys. *Materials Science and Engineering A, 354*(1-2), 121-132.

Kaya, C. (2008). Electrophoretic deposition of carbon nanotube-reinforced hydroxyapatite bioactive layers on Ti-6Al-4V alloys for biomedical applications. *Ceramics International, 34*(8), 1843-1847.

Kim, W. J., Hyun, C. Y., & Kim, H. K. (2006). Fatigue strength of ultrafine-grained pure Ti after severe plastic deformation. *Scripta Materialia, 54*(10), 1745-1750.

Kim, Y. H., Lee, J. M., & Hong, S. S. (2001). Optimal design of superplastic forming processes. *Journal of Materials Processing Technology, 112*(2-3), 166-173.

Kurzweg, H., Heimann, R. B., Troczynski, T., & Wayman, M. L. (1998). Development of plasma-sprayed bioceramic coatings with bond coats based on titania and zirconia. *Biomaterials, 19*(16), 1507-1511.

Kweh, S. W. K., Khor, K. A., & Cheng, P. (2002). High temperature in-situ XRD of plasma sprayed HA coatings. *Biomaterials, 23*(2), 381-387.

Lee, Y. S., Lee, S. Y., & Lee, J. H. (2001). A study on the process to control the cavity and the thickness distribution of superplastically formed parts. *Journal of Materials Processing Technology, 112*(1), 114-120.

Leventhal, G. S. (1951). Titanium, A metal for surgery. *The Journal of Bone and Joint* Surgery, 33(2), 473-474.

Liang, H., Shi, B., Fairchild, A., & Cale, T. (2004). Applications of plasma coatings in artificial joints: an overview. *Vacuum, 73*(3-4), 317-326.

Lin, K., Chang, J., Cheng, R., & Ruan, M. (2007). Hydrothermal microemulsion synthesis of stoichiometric single crystal hydroxyapatite nanorods with mono-dispersion and narrow-size distribution. *Materials Letters, 61*(8-9), 1683-1687.

Long, M., & Rack, H. J. (1998). Titanium alloys in total joint replacement – a materials science perspective. *Biomaterials, 19*(18), 1621-1639.

Lütjering, G., & Williams, J.C. (2003). *Titanium*, Berlin: Springer-Verlag.

Madusanka, W. A. P. S. (2009). Superplastic Forming. In *Latest News About Materials*. Retrieved January 3, 2011, from http://materialspro.blogspot.com/2009/02/superplastic-forming.html

Materials Evaluation and engineering, Inc. (2009). Energy Dispersive X-ray Specteoscopy. In Handbook of Analytical Methods for Materials. Retrieved April 19, 2011, from http://mee-inc.com/eds.html

Markovsky, P. E. (1995). Improvement of structure and mechanical properties of cast titanium alloys using rapid heat treatment. *Materials Science and Engineering A, 190*(1-2), L9-L12.

Nath, S., Tripathi, R., & Basu, B. (2009). Understanding phase stability, microstructure development and biocompatibility in calcium phosphate-titania composites, sybthesized from hydroxyapatite and titanium powder mix. *Materials Science and engineering : C, 29*(1), 97-107.

Nieh, T. G., & Wadsworth, J. (1997). Microsructural characteristics and deformation properties in superplastic intermetallics. *Materials Science and Engineering: A, 239-240*, 88-96.

Niinomi, M. (2002). Recent metallic materials for biomedical applications. *Metallurgical and Materials Transactions A, 33*(3), 477-486.

Nonami, T., Kamiya, A., Naganuma, K., & Kameyana, T. (1998). Implantation of hydroxyapatite granules into superplastic titanium alloy for biomaterials. *Materials Science and Engineering: C, 16*(4), 281-284.

Onoki, T., Hosoi, K., Hashida, T., Tanabe, Y., Watanabe, T., Yasuda, E., et al. (2008). Effects of titanium surface modifications on bonding behavior of hydroxyapatite ceramics and titanium by hydrothermal hot-pressing. *Materials science and Engineering: C, 28*(2), 207-212.

Orlovskii, V. P., Komlez, V. S., & Barinov, S.M. (2002), Hydroxyapatite and hydroxyapatite-based ceramics. *Inorganic Materials, 38*(10), 973-984.

Park, C. H., Ko, Y. G., Park, J. W., & Lee, C. S. (2008). Enhanced superplasticity utilizing dynamic globurization of Ti-6Al-4V alloy. *Materials Science and Engineering: A, 496*(1-2), 150-158.

Peters, M., Hemptenmacher, H., Kumpfert, J., & Leyens, C. (2003). Fundamentals and Application. In C. Leyens and M. Peters (Eds), *Titanium and Titanium Alloys* (pp. 1-57). Germany: Wiley-VCH.

Pilling, J., & Ridley, N. (1989). *Superplasticity in Crystalline Solids*. London: Institute of Metals.

Pleshko, N., Boskey, A., & Mendelsohn, R. (1991). Novel infrared spectroscopic method for the determination of crystallinity of hydroxyapatite minerals. *Biophysical Journal, 60*(4), 786-793.

Rabiei, A., Thomas, B., Jin, C., Narayan, R., Cuomo, J., Yang, Y., & Ong, J. L. (2006). A study on functionally graded HA coatings processed using ion beam assisted deposition with in situ heat treatment. *Surface Coatings Technology, 200*(20-21), 6111-6116.

Rack, H. J., & Qazi, J. I. (2006). Titanium alloys for biomedical applications. *Materials Science and Engineering: C, 26*(8), 1269-1277.

Ramdan, R. D., Jauhari, I., Hasan, R., & Nik Masdek, N. R. (2008). The role of strain rate during deposition of CAP on Ti6Al4V by superplastic deformation-like method using high-temperature compression test machine. Materials Science and Engineering; A, 477(1-2), 300-305.

Sanaz, Y. P., Iswadi Jauhari, Mohsen, A. Z. (2010). Implantation of HA into superplastic Ti-6Al-4V: Kinetics and mechanical behaviors of implanted layer. *Metallurgical and Transactions A, 42*(1), 219-226.

Semiatin, S. L., Seetharaman, V., & Weiss, I. (1999). Flow behavior and globurization kinetics during hot working of Ti-6Al-4V with a colony alpha microstructure. Materials *Science and Engineering A, 263*(2), 257-271.

Shibata, H., Tokaji, K., Ogawa, T., & Shiota, H. (1996). Microstructure dependence of fatigue strength and fatigue crack propagation in titanium aluminide. *International Journal of Fatigue, 18*(2), 119-125.

Sibum, H. (2003). Titanium and titanium alloys- From raw material to semi finished products. *Advanced Engineering Materials, 5*(6), 393-398.

Siegert, K., & Werle, T. (1994). Physical Mechanism of Superplasticity. In *TALAT Lecture 3802*. Retrieved May 12, 2010, from http://www.slideshare.net/corematerials/talat-lecture-3802-physical-mechanism-of-superplasticity

Song, W. H., Jun, Y. K., & Hong, S. H. (2004). Biomimetic apatite coatings on micro-arc oxidized titania. *Biomaterials. 25*(17), 3341-3349.

Sousa, S. R., & Barbosa, M. A. (1996). Effect of hydroxyapatite thickness on metal ion release from Ti6Al4V substrates. *Biomaterials, 17*(4), 397-404.

Taylor, J. C., Driscoll, C. F., & Cunningham, M. D. (1996). Failure of a hydroxyapatite-coated endosteal dental implant: A clinical report. *The Journal of Prosthetic Dentistry, 75*(4), 353-355.

Tian, Z. R., & Fulbright, J. W. (2008). Nanotechnology for improving bone implants. *Technology,* 76-80.

Thomas, M. B., Doremus, R. H., Jarcho, M., & Salsbury, R. L. (1980). Dense hydroxylapatite: fatigue and fracture strength after various treatments, from diametral tests. *Journal of Materials Science, 15*(4), 891-894.

Vanderhasten, M., Rabet, L., & Verlinden, B. (2005). High temperature deformation of Ti6Al4V at low strain rate. *Metallurgy, 11*(3), 195-200.

Wang, G. C., & Fu, M. W. (2007) Maximum *m* superplasticity deformation for Ti-6Al-4V titanium alloy. *Journal of Materials Processing Technology, 192-192,* 555-560.

Wang, K. (1996). The use of titanium for medical applications in USA. *Materials Science and Engineering: A, 213*(1-2), 134-137.

Wang, S., Lacefield, W. R., & Lemons, J. E. (1996). Interfacial shear strength and histology of plasma sprayed and sintered hydroxyapatite implants in vivo. *Biomaterials, 17*(20), 1965-1970.

Watari, F., Yokoyama, A., Omori, M., Hirai, T., Kondo, H., Uo, M., et al. (2004). Biocompatibility of materials and development to functionally graded implant for bio-medical application. *Composite Science and Technology, 64*(6), 893-908.

Wikimedia Foundation, Inc. (2011). Energy-dispersive X-ray spectroscopy. Retrieved April 19, 2011 from Wikipedia, the free encyclopedia.

Xiong, J., Li, Y., Hodgson, P. D., & Wen, C. (2010). Nanohydroxyapatite coating on a titanium-niobium alloy by a hydrothermal process. *Acta Biomaterialia*, *6*(4), 1584-1590.

Yoshimura, H., & Nakahigashi, J. (2002). Ultra-fine-grain refinement and superplasticity of titanium alloys obtained through protium treatment. *International Journal of Hydrogen Energy*, *27*(7-8), 769-774.

Zhang, S., Xianting, Z., Yongsheng, W., Kui, C., & Wenjian, W. (2006). Adhesion strength of sol-gel derived fluoridated hydroxyapatite coating. *Surface and Coatings Technology*, *200*(22-23), 6350-6354.

Zhao, Y. H., Liao, X. Z., Jin, Z., Valiev, R. Z., & Zhu, Y. T. (2004). Microstructures and mechanical properties of ultrafine grained 7075 Al alloy processed by ECAP and their evolutions during annealing. Acta Materialia, 52(15), 4589-4599.

# PUBLICATIONS

(1) S. Yazdan Parast, I. Jauhari, M. Asle Zaeem, A.H. Mohamad Dom, **H. Mohd Khalid** Embedment of HA into Superplastic Ti-6Al-4V: Effects of Implantation Temperature Advanced Materials Research Vols. 97-101 (2010) 3905-3909.

(2) Adibah Haneem Mohamad Dom, Iswadi Jauhari, Sanaz Yazdanparast, **Hidayah Mohd Khalid** Embedment of HA/Ti composite powder on superplastic titanium alloys (Ti-6Al-4V) Journal of Materials Science and Engineering A (2010) Volume 527, Issues 21-22, (2010) 5831-5836.